Journal Pre-proof

Palaeohydrology from the Northern Salado River, a lower Parana river tributary (Argentina)

Oscar Pedersen, Ernesto Brunetto, Daniela M. Kröhling, María BelénThalmeier, María Cecilia Zalazar

PII: S0895-9811(22)00336-4

DOI: https://doi.org/10.1016/j.jsames.2022.104050

Reference: SAMES 104050

To appear in: *Journal of South American Earth Sciences*

Received Date: 29 May 2022

Revised Date: 16 September 2022

Accepted Date: 22 September 2022

Please cite this article as: Pedersen, O., Brunetto, E., Kröhling, D.M., BelénThalmeier, Marí., Zalazar, Marí.Cecilia., Palaeohydrology from the Northern Salado River, a lower Parana river tributary (Argentina), *Journal of South American Earth Sciences* (2022), doi: https://doi.org/10.1016/j.jsames.2022.104050.

This is a PDF file of an article that has undergone enhancements after acceptance, such as the addition of a cover page and metadata, and formatting for readability, but it is not yet the definitive version of record. This version will undergo additional copyediting, typesetting and review before it is published in its final form, but we are providing this version to give early visibility of the article. Please note that, during the production process, errors may be discovered which could affect the content, and all legal disclaimers that apply to the journal pertain.

© 2022 Published by Elsevier Ltd.

Journal Pre-proof

Palaeohydrology from the Northern Salado River, a lower Parana River tributary (Argentina)

Oscar Pedersen[3,4], Ernesto Brunetto[3,4], Daniela M. Kröhling[1,2], María BelénThalmeier[1,4] and María Cecilia Zalazar[4]

1 CONICET, Argentina

2 FICH-UNL, Universidad Nacional del Litoral, CC 217, 3000 Santa Fe. Argentina

3 CICyTTP (CONICET-UADER-Prov. ER), Dr. Materi y España 149, 3105 Diamante, Entre Ríos, Argentina

4 LAGEO- FCYT-UADER, Universidad Autónoma de Entre Ríos, Entre Ríos, Argentina

ABSTRACT

Palaeofloods and drainage palaeostage can be approached from sedimentological, stratigraphical, geomorphological, geodetic and geophysical information. This allows us to supply pre-instrumental and historical data and to assess a particular flood-prone area. It has been proved that the study of Late Holocene fluvial sediments is valuable source to estimate $1x10^2$-$1x10^3$yr. scale occurrence and long-term recurrence of maximum events. The geological evidence of palaeofloods in lowlands in Central Argentina may reveal higher discharges likely occurred in the near past.

In this work, we attempt to identify sedimentological evidence of past floods in Late Holocene sediments from the northern Salado River (NSR), an important tributary of the lower Paraná River basin (Chaco-Pampean plain region). In the yr. 2003, the lower reaches of the NSR recorded an extreme flood event that provoked a disaster in Santa Fe, a city of 500,000 inhabitants located at the river mouth.

Considering the importance of this event, we developed a geomorphometry methodology for discriminating different levels of fluvial terraces and flood indicators in a representative area of the NSR, using multi-scale resolution Digital Elevation Model (DEM) data. Descriptions of flood-associated fluvial landforms and sedimentological stratigraphic attributes were performed in the field. High-resolution geodetic information and digital optical images were obtained from UAV photogrammetry, Ground Penetrating Radar (GPR) cross-sections were achieved and addressed to detect extreme flood evidence. A geomorphometric routine was applied to simulate the extreme flood scenarios, based on the data obtained from the field. The map resulting from the simulation was compared to satellite images recorded in the yr. 2003 extreme flood. A series of slackwater deposits and other palaeostage indicators (SWD-PSI) showed elevations higher than those reached over the yr. 2003 extraordinary flood (instrumentally recorded) and in the yr. 1914 historic flood event. The geomorphometric simulation of a flood event, calibrated from these diagnostic landforms, allowed us to extend the flood-prone area beyond the boundaries of the current active floodplain and channel. The integrative methodology enabled the mapping of areas potentially prone to flooding. The estimations of the discharges associated to the inferred palaeofloods could be 50-80% larger than the maximum events historically documented and instrumentally measured.

Keywords: Palaeofloods; Late Holocene sequence stratigraphy; Geomorphometry of terraces; Ground Penetrating Radar; UAV Geodetic palaeohydrological reconstructions.

Introduction

Extreme climate events have increased in frequency and intensity in the SE of South America since the yr. 1970s (Cavalcanti et al., 2015; Lovino et al., 2022). This intensifies the risks for urban settlements and agriculture and causes significant infrastructure damage and a decrease in livestock productivity in the Chaco-Pampean plain (Barros et al., 2015; Lovino et al., 2022). The geological record provides long-term information on the conditions and processes that can drive physical, ecological, and social systems into new states that may be irreversible within human time frames (Brovkin et al., 2021). In that sense, geological and botanical archives

can preserve evidence of exceptional floods going back centuries to millennia (St. George et al., 2020). The field of palaeoflood hydrology involves advances in Quaternary geology and fluvial geomorphology from indirect discharge measurements (Baker, 2013, 2008). Conventional hydrological discharge determination involves energy-based inverse hydraulic modelling of discrete palaeofloods, recorded in appropriate settings, such as slackwater deposits and other palaeostage indicators (SWD-PSI) (Baker, 2013, 2008). Benito et al. (2020) presented a review of palaeohydrological techniques for estimating the magnitude and frequency of past floods using geological evidence. Long series of floods obtained from historical and sedimentary records (palaeofloods) might be analysed to obtain centennial-length records of flood discharges. Modern flood gauging records typically lack a period of time long enough as to capture the full range of floods associated with longer-term climate change. Therefore, the stratigraphic records of palaeofloods provide excellent data for reconstructing the long-term behaviour of flood regimes (Leigh, 2018). Besides, modern hydraulic and hydrological models cannot be validated without the baseline flood data provided by sedimentary and geomorphological approaches (Baker, 2008; Benito and Hudson, 2010; Lastra et al., 2008). Current and previous palaeoflood research have focused on high-stage slackwater sediments (Benito and O'Connor, 2013; Bodoque et al., 2015; Kochel and Baker, 1988), which consist of vertical accretion deposits, preferentially found near the peak stage of palaeofloods, contained within bedrock gorges or near the valley edges (Benito et al., 2020). Overbank vertical accretion of sediments (slackwater deposits on floodplains and low terraces) can provide continuous records of past flood frequency (Leigh, 2018). Also, fluvial deposits can represent short-term intrinsic changes promoted by extreme events or anthropogenic causes (Thorndycraft et al., 2008). The whole data helps delineate flood-prone areas in broad alluvial valleys by mapping flood-related landforms and deposits, soil and plant associations, and other flood observations (Benito and Hudson, 2010). The strength of model projections for climate change and hazard zonation should be based on the information stored in the natural archives of Holocene palaeoflood records (Baker, 2013).

A palaeohydrological bound is located on a terrace or abandoned floodplain surface, at a high elevation, on which a palaeostage has not been sufficiently exceeded so as to modify its surface (non-exceedance discharge threshold) (Benito et al., 2020). A careful examination should be carried out in order not to underestimate the threshold of such non-exceedance indicators. Flood chronologies from several regions suggest that rapid climate changes tend to be associated with more frequent occurrences of large and extreme floods (Knox, 2000). According to the latest IPCC report (Jiménez Cisneros et al., 2014), there is broad scientific consensus that climate change will produce variations in flood patterns. Although past hydrological episodes produced no direct analogues for global change impacts, they can furnish guidelines for predicting future extreme conditions of the fluvial systems (Gregory et al., 2006).

Global studies that emphasize the palaeostage estimation of Holocene palaeofloods have been increasing recently in western North America, Europe, Israel, India, South Africa, Australia, and China (Baker, 2013; Baker 2020; Benito 2020). However, palaeohydrology works are scarce in South America, particularly in Argentina (Baker, 2013). South America is a critical region for palaeohydrological investigation, as it includes the largest river basin in the world and one of the largest expanses of tropical forest in the southern hemisphere (Baker, 2000). Despite that, there has been little development in quantitative investigations (Baker, 2020;

Benito, 2020) and only descriptive studies of Late-Quaternary palaeohydrology of large South American fluvial systems have been reported (Latrubesse, 2003). Thus, to understand the global climate context, it is essential to encourage palaeohydrological research in this region.

On the other hand, photogrammetry from drones or UAV (Unmanned Aerial Vehicles) applied to palaeohydrology enables us to make predictions based on the reconstruction of palaeohydrometric levels. The study of geological sections, high-resolution optical images, digital terrain models and 3D subsurface models, synthesised in a GIS platform, achieves an integrative synthesis to address extreme flood phenomena studies concerning global climate change (Pedersen et al., 2022).

In this work, we delineated flood-prone areas on a multi-criteria base. We include sedimentary descriptions, geomorphological mapping and geodetic measurements of flood-related landforms and low-terraces, stream gauge records, and historical evidence (documentary) in a representative fluvial system of the extensive lowlands of Central Argentina. This approach is supported by stratigraphic loggings on cut-banks and from a ground-penetrating radar (GPR) survey achieved over the floodplain of the northern Salado River (NSR), which is an important tributary of the Middle Paraná River Basin, one of the largest river basins in the world. The lower NSR is a typical lowland fluvial system characterised by a meandering channel and widespread floodplains, affected by frequent lateral migration or channel avulsion. The lower NSR basin underwent an accelerated expansion of cattle ranching and soybean crops, with high deforestation rates (sub-tropical broadleaf forest) along the fluvial belt.

In yr. 2003, a catastrophic flood event, which provoked ca. 160 deaths, 62,500 displaced people and caused huge economic damage, was recorded in the lower basin of the NSR (Santa Fe province). This catastrophe affected Santa Fe city, which has ca. 500,000 inhabitants and is located at the river mouth. This flood was considered an unprecedented event by local authorities and technicians. This case demonstrates that the traditional hydrologic/hydraulic engineering has not been enough to gauge the buildings of protection.

Study area

The lower basin of the NSR is situated in the most distal region of the Salado-Juramento fluvial megafan (SJRM), the second-largest megafan (204,747 km^2) of the Chaco aggradation plain (Thalmeier et al., 2021). The Chaco plain (840,000 km^2) occupies the Andean foreland of South America (eastern Bolivia, northern Argentina, and northwestern Paraguay).

The present-day fluvial belt of the lower NSR (1–2.5 km wide) comprises a sinuous, single-thread meandering channel (with asymmetric waves), flanked by levees throughout its length. In the associated floodplain there are oxbow lakes, meander scrolls, meander cut-offs, and swamps. The radii and widths of the abandoned meanders are similar or up to four times the radii of the existing channel. Downstream of the Salado and Calchaquí confluence, the NSR occupies a N-S fluvial valley, 4–10 km wide and 20 m deep. The present-day NSR belt (3 km wide) displays a meandering channel (50–70 m wide) bordered by well-developed levees that are partially breached by numerous crevasse channels and splays. According to FICH-INA (1998), the rate of average maximum vertical accretion of the levee was estimated at 5 mm/year after the 1930s. Frequent

swamps are extended along the adjacent active floodplain and connected with yazoo streams. Cut-off meanders, oxbow lakes, infilled oxbows, swales and scroll bars are common. Two generations of oxbow swamps are deduced by their planform (one of them with radii and width comparable to the present-day meanders, and the other, doubling them). A main fluvial terrace appears in some sectors (1–2 km wide). Near the river mouth, the NSR assumes an anabranching pattern characterized by sinuous channels and islands (Thalmeier et al., 2021).

The study area in the Manucho site (Figure 1) is a typical depositional site for the research of the NSR Late Holocene-Present fluvial sedimentation. This area is located ca. 60 km upstream of the NSR mouth, without the influence of the Paraná River floods. The fluvial plain there allows linking the vertical sections of the subsurface with the depositional forms that are preserved in the floodplain.

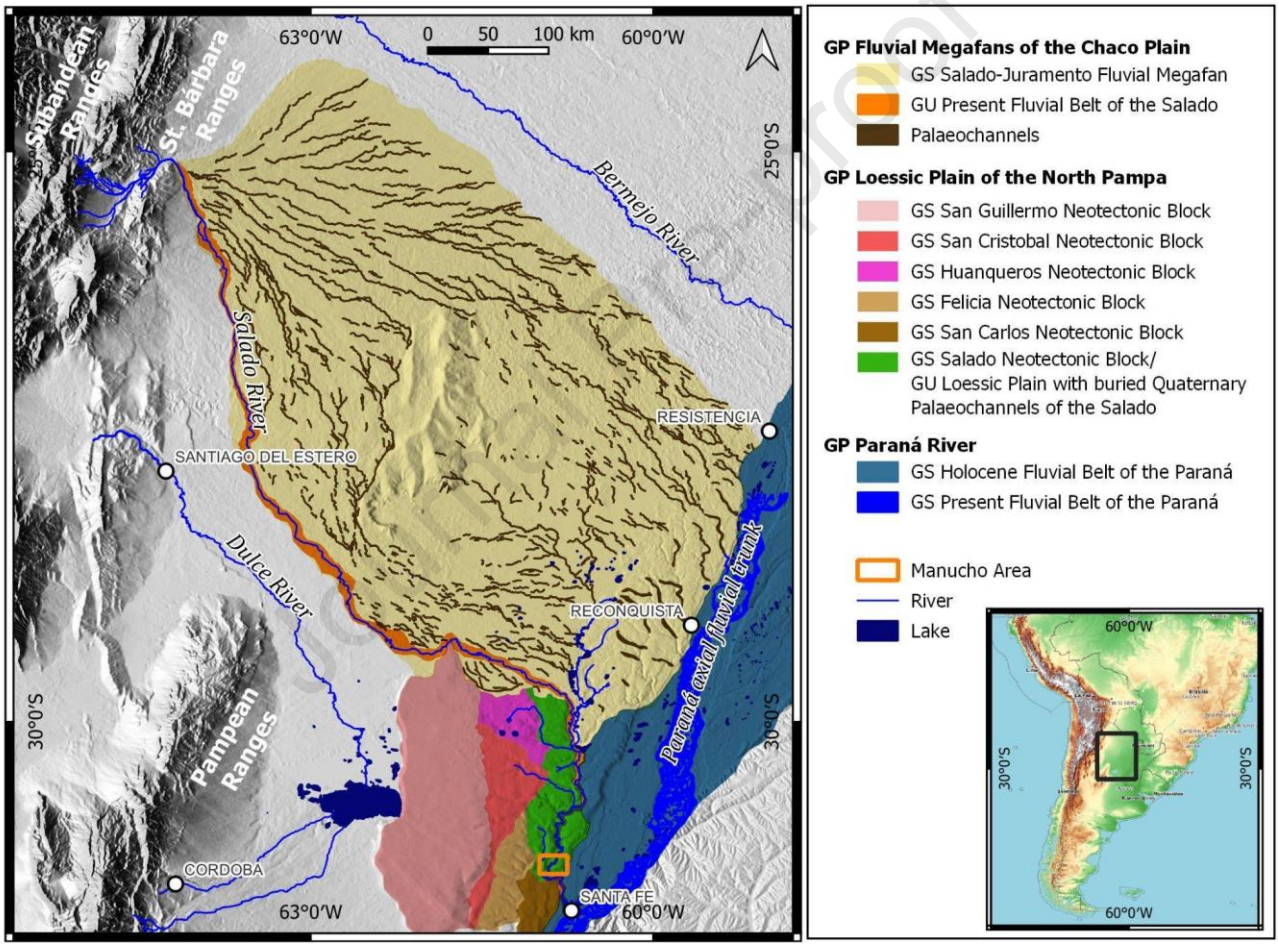

Fig. 1- Regional geomorphological map of the Salado-Juramento River Megafan (SJRM) and its lower river segment (NSR). This is part of a huge distributive fluvial system associated with the eastern Andean and Pampean foreland basins. The Parana River continental system is the trunk collector of the SJRM. GP: geomorphological province; GS: geomorphological system; GU: geomorphological unit;

Geological setting

The lower basin of the NSR (55.950 km^2 in Santa Fe province, Argentina) is specifically located in the broken foreland of the Pampean Ranges (Fig 1). This region is characterised by flat-slab subduction of the Nazca-Plate under the South American Plate (Ramos et al., 2002; Richardson et al., 2012). The present distal foreland basin that is occupied by widespread plains of the northern Pampa and southern Chaco can also be considered as a broken intracratonic crust. This internal cratonic dominium was affected by recent Quaternary deformation, evidenced by subtle positive morphostructures (Brunetto et al., 2019). These gently uplifted areas suffer present overflow erosion and stream incision. This region differs from the Bermejo and Pilcomayo fluvial megafans, southern Chaco, in that they produce overfilled foreland basins in a normal dipping slab subduction setting (Horton and DeCelles, 2001; Thalmeier et al., 2021). Unlike the Sub-Andean foreland basin, the Pampean broken foreland region generates a more complex distribution of depocentres and underfilled depozones.

Southern Chaco climate and hydrography

Chaco climate is dependent on the South American summer monsoon (SASM) (Vera et al., 2006; Zhou and Lau, 1998). This air circulation over tropical–subtropical South America in summer is regulated by low-latitude temperature differences between the continent and the oceans (Garreaud et al., 2009; Vera et al., 2006). As a regional response to the convective heating, a deep continental low is generated over the Chaco region (Ferrero and Villalba, 2019). The Chaco Low circulation and its interaction with the Andes intensify the moisture transportation from tropical to subtropical South America. The regional intensification of the eastward air circulation from the Andes is due to the South American Low-Level Jet (SALLJ). This circulation transports moisture that generates heavy convective rainfall. It occurs when the SALLJ moves along the eastern slopes from the Andes in summer over the subtropical plains as far south as 35°S (Garreaud et al., 2009; Saulo et al., 2004; Vuille et al., 1998). According to Garreaud et al. (2009), the amplitude of the El Niño Southern Oscillation (ENSO)-related anomalies can experience significant changes on decadal and longer timescales (through atmospheric teleconnections) over much of subtropical South America. EN episodes are associated with wet conditions in the SE part of the continent, with periodicities between 3 and 6 years. In general, ENSO is related to a significant increase in precipitation and river flow over the region, which conducted a “climate shift” around the 1970s/1960s (Garreaud et al., 2009; Lovino et al., 2022).

The Chaco area presents a tropical humid to tropical semi-arid climate from E to W (Iriondo, 1993). Considering the 1981–2010 series, the annual precipitation presents an E–W gradient, with rainfall amounts ranging from 1500 mm/yr towards the east to 800 mm/yr towards the west (Lovino et al., 2022). According to the precipitation spatial gradient, the lower NSR basin is located in the Humid Chaco (900–1,500 mm/yr).

The Salado-Juramento River flows about ca. 1,500 km from the Sub Andean Ranges (with its headwaters at 4,895 m asl) to its mouth at the Paraná River (25 m asl) in the Chaco/Pampa Plain transition. The SJRM has a very low regional slope and high discharge variability. Modern river channel patterns vary downstream changing from braided at the fan apex to meandering in the distal zone of the megafan. The active fluvial belt adjacent to the distal SJRM flows through its southern margin with a NW-SE direction. A large seasonally

flooded plain develops in the distal area of the megafan, crossed by palaeofluvial belts of the SJRM. In this area, large swamps form the headwaters of a local river network, the Golondrinas/Calchaquí meandering system. This is the main tributary to the current lower segment of the NSR. Many authors have reported river discharges at different gauging stations along with the river's flow. In the Andean segment of the river (at the Cabra Corral gauging station), a mean discharge of 29.5 m3/s was referred by Spalletti and Brea (2002). At the exit point of the Juramento River from the mountain front (El Tunal gauging station), a mean annual discharge of 42 m^3/s (yrs. 1941 to 1986) was measured, with mean discharges of 70.9 m^3/s (December to April) and of 22 m^3/s (May to November) (Cafaro et al., 2009). The mean monthly discharges recorded in the humid months exceed 110 m^3/s, with daily discharge peaks reaching 1,170 m^3/s (Secretaría de Estado de Energía-Agua y Energía Eléctrica, 1970). At the most downstream gauging station (Route 70), the NSR mean annual discharge ranges from 100 to 250 m^3/s, with peaks of 430 to 660 m^3/s (yrs. 1954-2016) (Secretaría de Infraestructura y Política Hídrica de la República Argentina, 2022). In the extreme humid period in 2003, the maximum discharge of NSR recorded in Santa Fe city reached an average daily discharge of 4,000 m^3/s, causing a catastrophic flood. The High rainfall over a saturated lower basin of the NSR was the main cause. Seasonal and interannual hydrological changes generate variable discharge regimes and exceptional flood events. The recurrence time for extraordinary RS flood (4,000 m3/s) for the period 1971-2003 is ca. 100 years (Paoli et al., 2015).

Materials and methods

In order to address a multicriteria approach to the palaeohydrological problem, geomorphological and stratigraphical principles and techniques were applied (Appendix 1). Fluvial landforms were identified from satellite images combined with geomorphometric procedures derived from 5 m and 30 m Digital Elevation Models (DEM) (Instituto Geográfico Nacional, 2021). A time series of satellite images was examined, searching extreme flood events from Earth Observing-1 (EO-1) and Landsat-7sensors. The images were downloaded via https://earthexplorer.usgs.gov (USGS EarthExplorer Data). A geomorphometric routine was run under GRASS-GIS free and open source software (GRASS Development Team, 2022).

Calibration of digital elevation models

To achieve the geomorphometric processing, we employed two DEMs, MDE-Ar 30m v2.1 and MDE 5m, produced by the Argentinian National Geographic Institute (Instituto Geográfico Nacional, 2021). These products resulted from the integration and processing of altitude data obtained by SRTM and ALOS satellite missions and local aeroplane photogrammetric flights. IGN reported a whole vertical resolution of 2 m for MDE-Ar 30 m v2.1 and a sub-metric vertical resolution for DEM 5 m. In order to validate these altitude data, we employed 11 high precision elevation control points from the High Precision Levelling Network of Argentina (Instituto Geográfico Nacional. Dirección de Geodesia, 2017; Instituto Geográfico Nacional, 2021), spatially distributed in the study area and referenced in the National Vertical Reference System (SRVN16). As the DEM 5 m contains null data in the fluvial belt zone at the bottom of the fluvial valley, we merged both

products (30m and 5m) by means of the r.mblend of the GRASS GIS routine. This produced a smooth transition from the high-resolution DEM (5m) to the low-resolution DEM (30m).

We used the module DTM Filter (slope-based) in SAGA GIS to classify its cells into bare earth and object cells (ground and non-ground cells). From this, we tried to minimise the presence of objects in the cover (vegetation and buildings), to represente a bare surface of the ground (Vosselman, 2000).

An estimation of the exactitude was obtained by calculating RMSE and deviation between altitude values of the DEM and their corresponding altitudes from the high precision network (SRVN16). Statistics from residual values (z_{DEM}-z_{SRVN16}), mean difference, standard deviation, minimum and maximum, were considered for corrections and examination of the precision of the altitude values. For correction and improvement of the data quality, the mean difference of residual values was subtracted from MDE-Ar 30m. Some improvement can be observed by diminishing the recalculated RMSE (2.2186m; Table 2). For the blended and filtered DEM (DEM 5m) we computed a RMSE of 1.1962m (Table 2).

To estimate the altitudes of the main flood indicators studied in the field, the HD DEMs derived from UAV surveys across the fluvial valley were also calibrated and corrected. The vertical precision was enhanced by the subtraction of the mean residual differences by comparing with the DEM previously calibrated from the high precision network (SRVN16) (Table 2). RMSE values below 1m were computed for these products (Table 2).

DEM	MIN DIF	MAX DIF	MEAN DIF.	σ	RMSE
MDE-Ar 30m	-0.4926	58.554	12.652	21.601	29.136
MDE-Ar 5m	-0.8120	12.272	0.4377	0.6419	10.873
Calibrated MDE-Ar 30m	-17578	42.577	12064	17791	22.186
Blended DEM 5m	-0.9230	14.292	0.6397	0.8219	11.962
VANT 1	-21501	-0.9303	12275	0.4858	13.307
VANT 2	-12300	0.7600	0.4453	0.6352	0.6202
VANT 3	44891	62.505	56587	0.6585	57.589
Calibrated VANT 1	-10800	0.1501	0.1844	0.4174	0.8687
Calibrated VANT 2	-0.6000	0.3000	0.1609	0.2922	0.4308
Calibrated VANT 3	-0.8623	11.707	0.3235	0.7020	0.7149

Table 2 - DEM calibration statistics

Geomorphometry of terraces and flood levels

We elaborated a series of geomorphometric raster maps from the DTM. These results consisted of slope and analytic relief maps, a simulated stream map based on a multiple flow direction accumulation script, the extraction of the main channel (raster and vector formats), and a landform map based on the slope association types (r.geomorphon; Jasiewicz and Stepinski, 2013).

The main prospective procedure that enables the identification of SWD-PSIs consists of automated methods to extract remnant terrace surfaces from DEMs. For this, we adapted procedures previously proposed for low-land areas (del Val et al., 2015; Demoulin et al., 2007; Józsa, 2019). This resulted in two products. One of

them was based on the tool generated by the GRAS-GISS platform for delimiting the remnant terrace surfaces by applying the algorithm r.terrace.geom (Józsa, 2019). This algorithm determines the cells that potentially correspond to fluvial terraces in function of local slopes and relative elevations, with respect to the main channel. It also produces statistics that describe the extracted terrace surfaces. Longitudinal profile, swath profile and frequency histogram of relative elevation from the fluvial channel describe discrete terrace surfaces. The second product was achieved by applying the algebra of maps. A map raster calculator was used to run a routine that intersects ranges of relative elevations and slopes lesser than a threshold of one degree. The map algebra computation was constrained to a 2.5 km wide belt from the main channel of the NSR toward both sides. Because of the low slopes of the channel, relative elevations of terraces were referred to the lowest elevation of the channel downstream to the end of the analysed belt. On the basis of regional stratigraphic correlation with dated lithostratigraphic units of the Chaco-Pampa plains (Thalmeier et al., 2021), we assumed the lowest terraces nearest the stream channel to be of Late Holocene age.

Classification and mapping of fluvial geomorphological units were based on typical landforms of sand-bed alluvial rivers following Leopold et al. (1964), among others.

A GRASS-GIS-based methodology for flash flood hazard assessment (Suprit et al., 2010) was implemented as an expedited mode to simulate extreme events. The method searches for identifying low-lying areas from DEMs. It predicts and delineates the areas nearest the stream channel, the ones most likely to be affected by flash floods (flood-prone areas). We adjusted the computational parameters to evidence of instrumental-recorded extreme floods from satellite images and correlations of hydrometric measurements from gauges. We attempted to reconstruct palaeoflood levels below the non-exceeded flood threshold. To this, we calibrated the low-lying areas simulation from the mapped terrace surfaces.

Fluvial stratigraphy and sedimentology

Fieldworks comprised analysis of outcrop 2D representation of sections drawn in natural NSR cuttings. Annotated sketch sections showing all the main sedimentological features, allowing a first 3D analysis of the depositional architecture of the NSR (vertical facies associations, bedding, cross-stratification, bounding surfaces, and architectural elements) were drawn, supplemented by photographs (Miall 1977; Allen,1983; Collinson, 1996; Bridges and Castle, 2003; Nichols, 1999). Graphic logs were drawn in selected 1D-profiles recording sedimentological data that describe the main fluvial forms. We focused on those indicating palaeoflood evidence, limited by clues of sedimentary stability stages such as pedogenic features.

Boreholes were done by a manual auger, with descriptions of sediment texture and pedofeatures (Catt et al., 1990). Mineralogical analysis (loose-grain technique) of sedimentary samples from boreholes was performed on the very fine sand fraction (63-125 μm) applying orthoscopic and conoscopic methods with a polarising microscope, using eugenol as an immersion liquid (n=1.54).

Stratigraphic analyses using GPR

Ground penetrating radar (GPR) is a near-surface geophysical technique based on the emission and reception of high-frequency electromagnetic waves which propagate into the subsurface. The application of geophysical

techniques such as GPR has made it possible to establish in more detail the internal architecture of the modern fluvial system, which helps to establish the mechanisms that generate sets of strata (Bristow et al., 1996, 2000). Near-continuous GPR cross-sections may reveal the complete 2D or 3D dimensional geometry of the sediment body and enable the quantitative determination of a fluvial channel depth and width. Thus, some of the GPR sections were located above sedimentary sequences outcropping at the NSR channel enabling detailed verification, particularly the analysis of architectural elements. The GPR sections crossing the identified Holocene fluvial terraces were verified by augering. 7.12 km of GPR profiles were recorded using a pulse EKKO equipment composed of two antennas (transmitter and receiver) of 250 MHz frequency with a coupled odometer, a control unit and a microcomputer monitor. This allowed us to investigate depths of up to 5 m in the study area. Depth-conversion velocities of 0.15 m ns-1 (unsaturated sediments) and 0.06 m ns-1 (saturated sediments or clays) were derived from isolated CMP tests, standard tables and water tables in the vicinity of the river channel. However, the depth reached by the GPR did not reach the water table. Standard data processing was applied to the recorded sections, using pulse EKKO software. This included infilling of missed traces, removal of the instrument noise using a high-pass filter, removal of a background ringing signal by the subtraction of a mean trace averaged over adjacent traces and topographic correction.

Geodetic survey. UAV photogrammetry for palaeohydrology

Photogrammetry with real-time correction was used here as a tool to access the sites, to survey fluvial landforms using HD images, and to produce digital surface, digital terrain and sectorised 3D models.

UAV images were georeferenced by visual analysis in a given local context or processed by indirect referencing through ground control points (GCP) acquired by geodetic differential receivers (GNSS) (Gabrlik et al., 2016). The use of real-time kinematic positioning (RTK) allowed us to improve the accuracy of the GNSS receiver on-board the drone, by means of a correction signal sent by a base station.

Flight planning and image acquisition

Flight missions were conducted over the study areas using a DJI Phantom 4 RTK (P4RTK; DJI) and a DJI Phantom 4 Pro v.2 (P4PRO; DJI) (Table 1). For the flights conducted with the P4PRO, Pix4Dcapture software (Pix4D, Version 4.12.1) installed on a Smartphone S61 of Caterpiller (Model CS61SBBNAMUN) was used to conduct the flight missions. The P4RTK flights used the on-board mission control software as provided with the sUAS and the configurations with RTK GPS activated (RTK enabled). The initial flights of the prospecting-scale field and the detail-scale field were conducted on 07 Nov. 2018. An additional set of flights of the detail-scale field were also performed on 20 Nov. 2021 to provide a validation dataset using the P4RTK with RTK enabled (Table 1).

All flights of the detail-scale field were conducted using P4RTK at one above ground level altitude (AGL): 100 and 120 m. To ensure that photogrammetry software could accurately process the images, the front and side image overlap was set at 80%. For the prospecting-scale field, flights were conducted with the P4PRO at altitudes 120 m AGL, with side and front image overlaps set at 80%, during an operational window spanning

3 h before and after solar noon on cloud-free days to minimise solar zenith angle, maximise illumination, and minimise shadows.

UAV	Field	RTK	GCP	Altitude m (AGL)	N° of Images	Flight date
P4PRO	Prospecting-scale	N/A	10	120	1587	7 Nov. 2018
P4RTK	Detail-scale	Enable	2	120	238	20 Nov. 2021
P4RTK	Detail-scale	Enable	2	100	321	20 Nov. 2021
P4RTK	Detail-scale	Enable	2	100	209	20 Nov. 2021

Table 1 – UAV Flight Plan

Georeferencing of UAV photogrammetric blocks

A large number of fixed-wing and multi-copters UAV on the market today include the so-called RTK option, where an onboard multi-frequency GNSS receiver can determine the camera position at shooting time with cm-level accuracy thanks to differential corrections sent by a master station or through the ground control station by a Continuously Operating Reference Station (CORS) network (Forlani et al., 2019).

Photogrammetric data processing

Photogrammetric data processing was executed with the commercial package Agisoft Metashape Professional version 1.7.4, build 12821, by Agisoft LLC, St. Petersburg, Russia. Block orientation is performed with SfM algorithms in an arbitrary reference frame.

The general workflow in Metashape progressed in five general steps: (a) tie point cloud construction, (b) GCP placement and camera optimization, (c) dense cloud construction, (d) DEM construction, and (e) generation of the orthomosaic. The tie point cloud, also referred to as the sparse point cloud, was constructed by aligning the photos with the key point, and tie point limits increased from the default levels of 40,000 and 4,000 to 200,000 and 20,000, respectively. Once GCPs were placed in each scenario, they were identified in at least two images to ensure that the software could automatically identify their position in all other images in which they occurred. Once all GCPs were placed into the scenario, cameras were optimised based upon the GCP locations to correct for spatial error in the rematching and optimization process. To accomplish this, all the cameras were deselected and GCPs were selected before optimization was used. To attempt to match the default settings for the generation of all Mesh 3D maps in high quality, the dense cloud was processed at medium quality with aggressive depth filtering. Once the dense point cloud was constructed, a DEM was produced using the dense point cloud with interpolation enabled and filtered to confidence. The orthomosaic was based on the DEM and was processed using the mosaic blending mode with hole filling enabled. The DEM and final orthomosaic were both constructed using the same Argentine Geodetic Positions 2007

(POSGAR07) official projection as the rest of the georeferencing scenarios in this study (SRVN16/POSGAR07 Zone 5).

Modelling overview

A workflow was generated starting with 3D geological modelling using Leapfrog Geo (Seequent Ltd. 2022). Leapfrog Geo is designed for rapid implicit modelling. The 3D mesh generation in Leapfrog Geo is based on contact surfaces that define the upper and lower limit of the unit. The interpreted stratigraphy, which defines the relative age of the units, affects the behaviour of the defined contacts. Leapfrog Geo offers three types of contact surfaces: Deposits contact, erosive contact, intrusion contact and vein contact (Seequent Ltd. 2022). The contact surfaces of the 3D geological model were generated with the first two types. The FastRBF interpolation method of Leapfrog Geo, which resembles the kriging method, was used to generate the contact surfaces. Geological models (GM) were constructed from surface maps, high-resolution geodetic, GPR and drilling data. Two models (GM1 and GM2) with similar stratigraphic distributions were generated in this study. Both GMs are a full 3D model that includes the sedimentary units that exist in the immediate vicinity down to 5m average depth.

Multi-temporal satellite image analysis of floods

The optical satellite images showing the most extreme flood episodes, selected from Earth Observing-1 (EO-1) and Landsat-7 sensors, were correlated to geodesic data recorded from the drone surveys. The results were compared with hydrometric measurements obtained over the yr. 2003-flood event. In turn, these data were correlated to geodesic positions of the terrace surfaces, mapped from the geomorphometric analysis and fieldwork control.

Historical record analysis

The maximum peak flood discharge from the instrumental record of the SRN occurred on the 8th of May, 2003. A report from technical institutions (MAH-UNL, 2006; pp 43) presents hydrological modelling of the yr. 2003 flood peak, based on pluvial measurements and the altitude-discharge curve. This curve was constructed from the fluvial section geometry at the water level gauge of route 4 (Manucho site), based on the local catchment area. The applied fitted curve is:

$$h > 10.36 \text{ m: } Q = 897.20316\, h - 8465.974 \quad (11)$$

h: altitude of hydrologic scale (MAH) [m], Q: Discharge [m^3/s].

The absolute elevation of the scale base is 13.28 m.a.s.l. (MAH).

We applied the proposed model to estimate inferred discharges based on geodetic data from SWI-PSI identified in the field.

Journal Pre-proof

Results

1. Fluvial geomorphology

The geomorphological classification presented in Figure 1 is based on the genetic landform type organised into hierarchical taxa. The highest level is represented by three geomorphological provinces (GP). The next level corresponds to geomorphological systems (GS), each of them comprising genetically linked geomorphological units (GU). The GS Salado-Juramento Fluvial Megafan (Thalmeier et al., 2021) includes the GU Present Fluvial Belt of the NSR. The tributary sub-basins on the right margin of the NSR fluvial belt cover large areas and belong to the GP Loessic Plain of Northern Pampa. Its GUs are morphostructural units because they were mainly shaped by Quaternary tectonic deformation. The San Guillermo elevated block is the main regional morphostructure, limited by fault systems (Brunetto et al., 2017). Moreover, the GS Holocene Fluvial Belt of the Parana, adjacent to the left margin of the NSR, is represented by GUs dominated by fluvial landforms.

In the study area (Manucho), a Holocene meander belt occupies a wide floodplain bordered by aggradational fluvial terraces (Fig. 2). The meander belt is mainly build-up by natural levees, crevasse splays and scrollbars. On the inner bend, fine sands are deposited by lateral accretion on the point bar scrolls and in the swales. Also, part of these landforms is covered by younger overbank deposits (levee or floodplain area). Crevasse splays resulting from overbank flow and partial breaching of levees during flood-stage conditions are common in the floodplain of the lower segment of the NSR, and particularly in the studied segment of the meandering river, dominated by a high curvature of the flow. Rectification of meanders is, in general, originated by avulsion due to crevasse splay progradation. The enrichment of fine sediments (mainly silt and very fine sands) during the overbank flood is the main process of accretion of the floodplain along the area throughout crevasse splays and overbank sheets of fine materials.

Recent chute cutoffs of the river channel by bank incision shifted the flow direction during extreme discharges (Fig. 2). Overbank sandy materials associated with these chute channels partially drowned palaeocrevasse channels and lobes generating a complex pattern. The main characteristics of the field of the preserved inactive crevasse channels are a series of aligned elongated hollows, each of them 45/50 m long and 11/17 m wide, with concave bottom limited by lateral high-gradient slopes (75°) and convex slopes (30-40°) at both ends. The adjacent crevasse lobes parallel to the elongated series of hollows are 0.50 m wide, with irregular convex topography and local topographic variations ranging from 0.20 to 0.30 m. These crevasse channels and lobes are covered by herbaceous vegetation. The Late Holocene fluvial levee (35/40 m wide) separates the palaeocrevasse channel hollows from the present NSR channel. Tributary rills dissect terraces, previously flowing to the floodplain and joining the main channel.

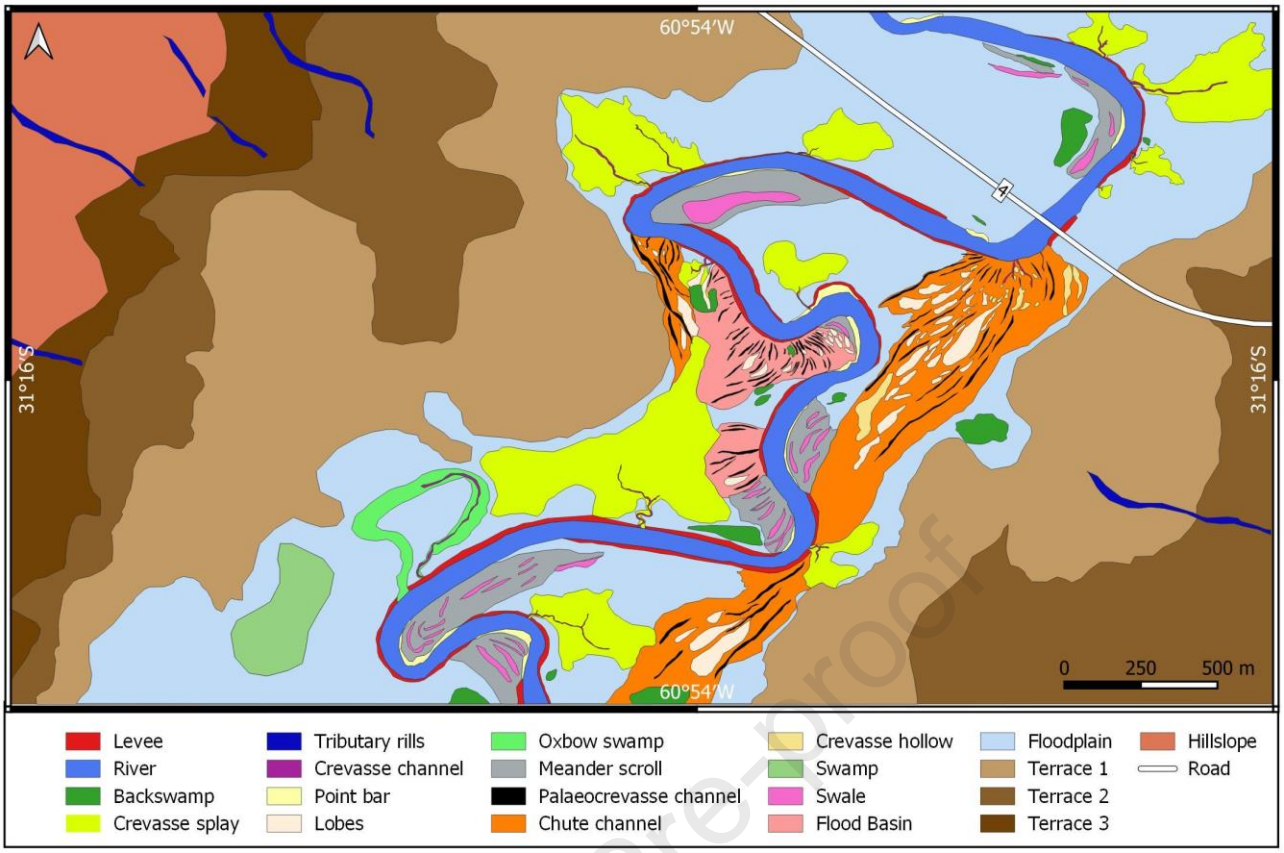

Fig. 2- Geomorphological map of the NSR valley in the Manucho area. For the location, see Fig. 1.

2. Mapping of terrace levels and reconstruction of flood hydrological levels

A remnant fluvial terrace zone is able to be identified and its approximated boundaries are mapped from the applied geomorphometric processing. This area is clearly recognisable on the right fringe of the river valley from the extraction process (Fig. 3). Discrete flat surface staircases may discriminate inside this general terrace zone. Relative elevations with respect to the watercourse level reach 2 to 8 m (Fig. 3). The most frequent relative level is 3 m with respect to the water level of the main channel. The surface ranging from 2 to 3 m above the watercourse level corresponds to the most active floodplain, and the relative elevations ranging 3-4 m, 5-7 m, 7-9 m and 14-16 m are related to discrete terraced surfaces, labelled T1, T2, T3 and T4, respectively (Fig. 3). They represent simulated hydrological levels, which allow us to map reaches prone to flooding. The risers between staircases of the fluvial terraces are highlighted from the geomorphon processing (Appendix 2). The boundaries between flat fluvial surfaces are highlighted from aligned associations of slopes: lineal ridges (vermillion red) adjacent to elongated low areas (blue). The combination of independent DEM geomorphometric processing, terrace extraction and geomorphon justifies the delineation of the boundaries of active floodplain and discrete fluvial terraces. The higher and older terrace surfaces (T4 and other) are smooth, because the risers became in washing slopes. T4 corresponds to the Pleistocene terrace, capped by a loess deposit.

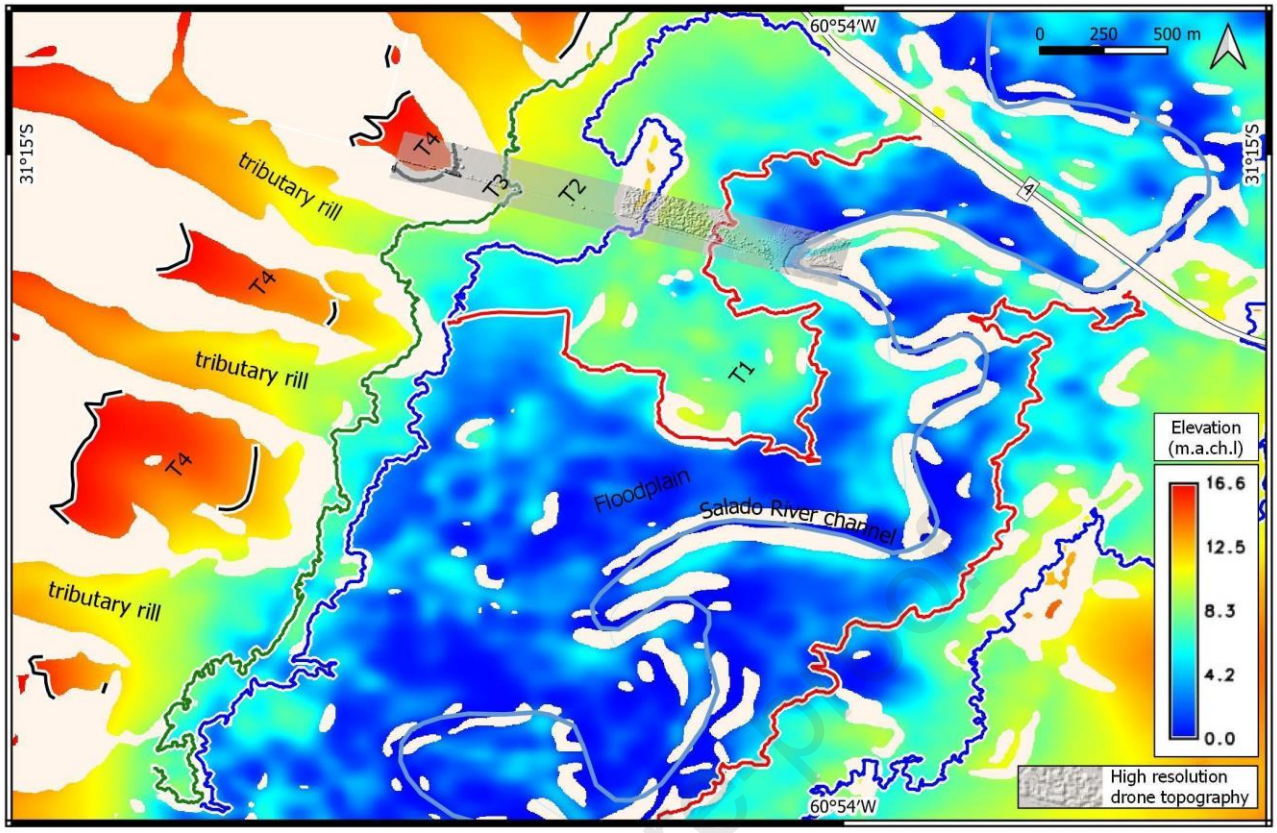

Fig. 3- Geomorphometric map of floodplain and terrace surfaces of the NSR in the Manucho area, derived from 5m DEM and calibrated from the high precision network (SRVN16). A grey transverse belt indicates the area surveyed by drone to obtain a high-resolution swath cross-section of the river valley. The mapping of terraces makes it possible to estimate flood-prone areas and simulated extreme hydrological scenarios, not-expected from the instrumental record.

Graphical R-statistics obtained from the procedure by Jodza (2019) display elevation levels of discrete terraces, which can be associated with potential extreme hydrological levels (Fig. 4). These levels represent T1 and T3 (ca. 3-4 m and 7-8 m above the watercourse, respectively).

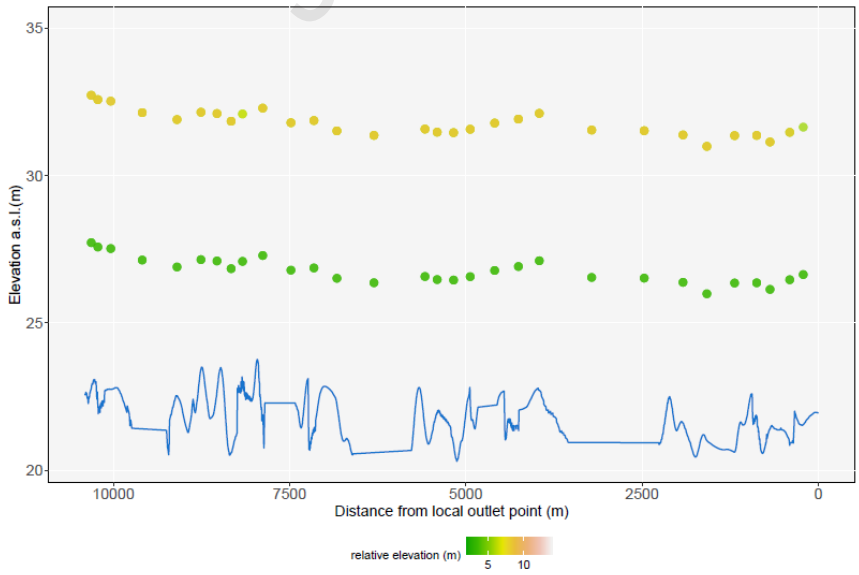

Fig. 4– Terrace-like surfaces along with the longitudinal profile of the NSR watercourse in the Manucho stretch, applying the script by Jodza (2019). The extraction of relative elevations from discrete terrace levels

enables us to estimate potential discharge magnitudes. This automated procedure displays at least two hydrological high stages in the study area (ca. 3-4 m and 7-8 m, above the watercourse).

3. Fluvial stratigraphy and sedimentology

3.1. Holocene sedimentary sequences outcropping along the main channel

The representative profile is located in the stratigraphic section on the concave erosional bank of the meander bend (31°15'18.84"S, 60°54'3.98"W; Fig. 5.1). A Holocene sequence covers silty-sand sequences, dated in the region as Late Pleistocene (Kruck et al., 2011)). The lower section of the Holocene profiles is formed by a silty-clayey bed (0.09 m thick) very dark grey (7.5YR 3/1) in colour. It contains few very fine Fe oxide motes. It is covered by a pale brown (10YR 6/3) very fine laminated sandy bed (0.05 m). A very dark-grey (7.5YR 3/1) silty-clayey bed (0.82 m) overlies it. It is structured in coarse peds, with frequent root moulds covered by cutans (10YR 2/2), few very fine Fe/Mn-oxide/hydroxide nodules, and few very fine micropores. It has fine to very fine sand-filled tunnels (crotovines). Archaeological remains were collected in the upper half of the stratum. This is a clay oven that was found in the Bt horizon of the paleosol (Fig. 5.2). Because of the observed pedofeatures, it is interpreted as a Bt horizon of a buried soil (Fh-FB; Fig. 5.2). The upper Holocene section overlies unconformably and begins with a pale brown (10YR 6/3) very fine silty sandy bed (0.45 m), poorly laminated and containing few root moulds. A laminated bed composed of very fine sand (0.40 m thick), very pale brown (10YR 7/3) in colour, and with few very fine Fe-oxide mottles overlies it. It is capped by fine to very fine laminated and micaceous sand (0.10 m thick), very pale brown (10YR 7/3) in colour, and containing few very fine Fe-oxide mottles. A very pale brown (10YR 7/3) fine laminated sand (0.03 m) overlies it. A yellow (10YR 7/6) fine to very fine laminated sandy bed (0.17 m), with few fine Fe-oxide mottles and micas, ends the outcropping profile. It is partially affected by present pedogenesis.

From the 2D stratigraphic cross-section of the outcrop where the sedimentological profile was logged (Fig. 5.1), we recognised a succession of macroforms characterised by the dominance of channel architectural elements at the base. They form channel belts composed of bedforms and bars, displaying high lateral variability. They consist of composed bars and channels that enumerate sand bed macroforms (SB) and frequent lateral accretion macroforms (LA). As a set of channel architectural elements, these units could be associated, composing large-scale complex sheets and large-complex ribbons (Veiga et al., 2007). They display storey scouring surfaces bounding SB and LA macroform associations (Fig. 5.2).

More hierarchical bounding surfaces limit the base of channels that were accumulated by long-term geomorphic processes (10^2-10^3yr) or longer sedimentary cycles (10^4-10^5yr) (Fig. 5.1). They are represented by order 5th and order 6th bounding surfaces, respectively. The main surfaces limit the Late Pleistocene – Holocene cycles and, likely, internal sedimentary cycles in the Late Pleistocene. The Holocene succession presents remarkable surfaces bounding the large-scale complex macroforms and storey channels limited by order 5^{th} surfaces at the base and order 4^{th} surfaces, bounding the accumulated macroforms. Internal accretion inclined surfaces (order 3^{rd}) correspond with the growth of macroforms, i.e., the progress of LA macroforms, from episodic inter-annual floods.

Journal Pre-proof

We interpret that this sequence represents a filling of a channel after avulsion or lateral migration of meandering channels. This sequence was followed by the accumulation of levee sediments. The vertical succession is characterised by alternating processes of erosion. Levees are eroded by action of crevasse splay channels over rising pulses. Channels are subsequently filled over falling and waning flows. The upward coarsening grain size trend of the sand beds would indicate increasing energy of the overbank flood flows. Therefore, the upper levee/crevasse splay sequence is representative of the active flood regimen. This record allows us to assess palaeoflood history.

Journal Pre-proof

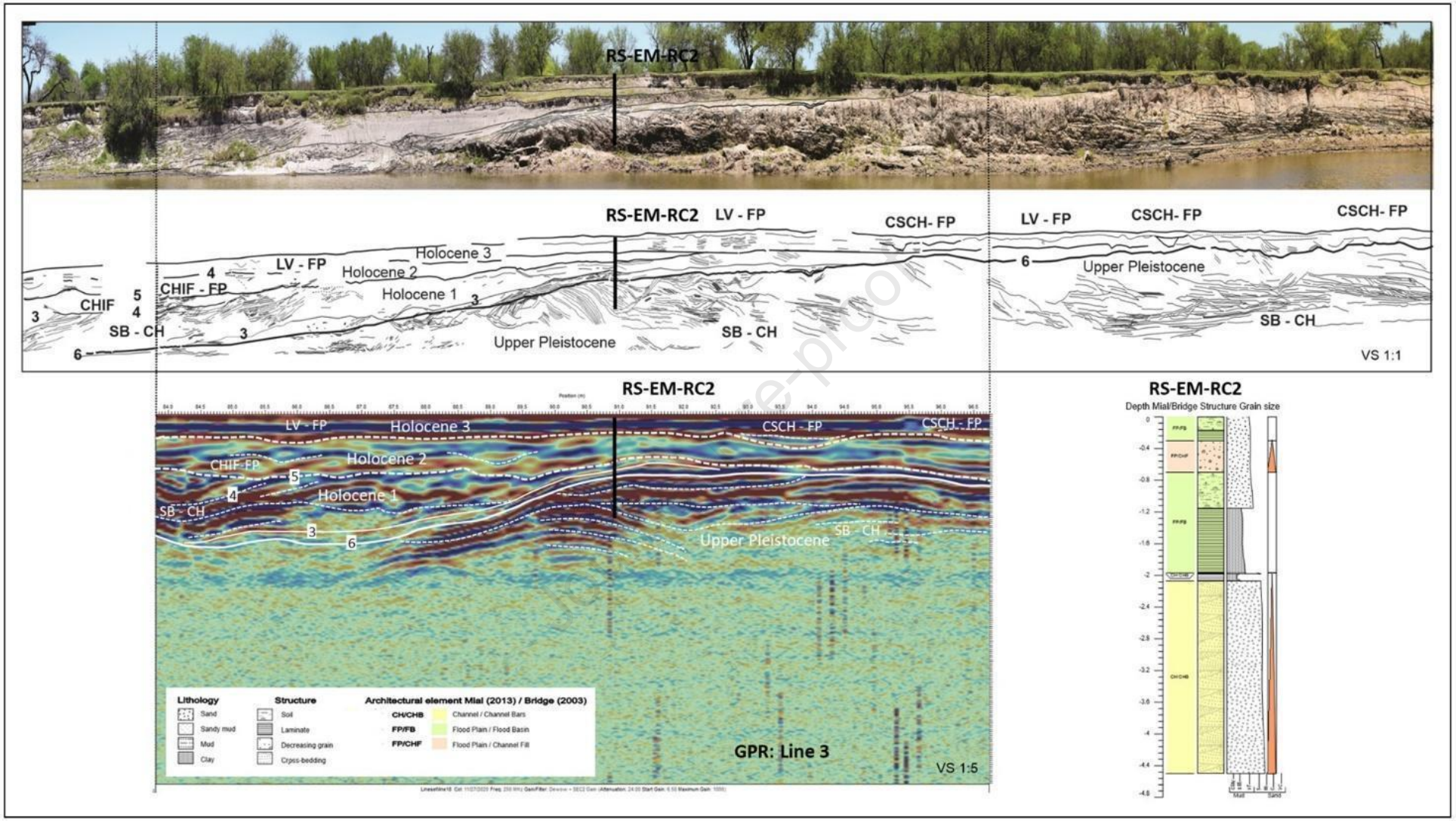

Fig. 5.1- Stratigraphic sequence section and sedimentological profile. From the outcrops and GPR sections, we interpret that the upper sequence (Holocene 3) contains the representative SWI-PSIs, comparable with the instrumental hydrological record. This sequence capped the sequences of migration or avulsion of the main channels, processes that formed the base of the present floodplain and recent surface of terraces.

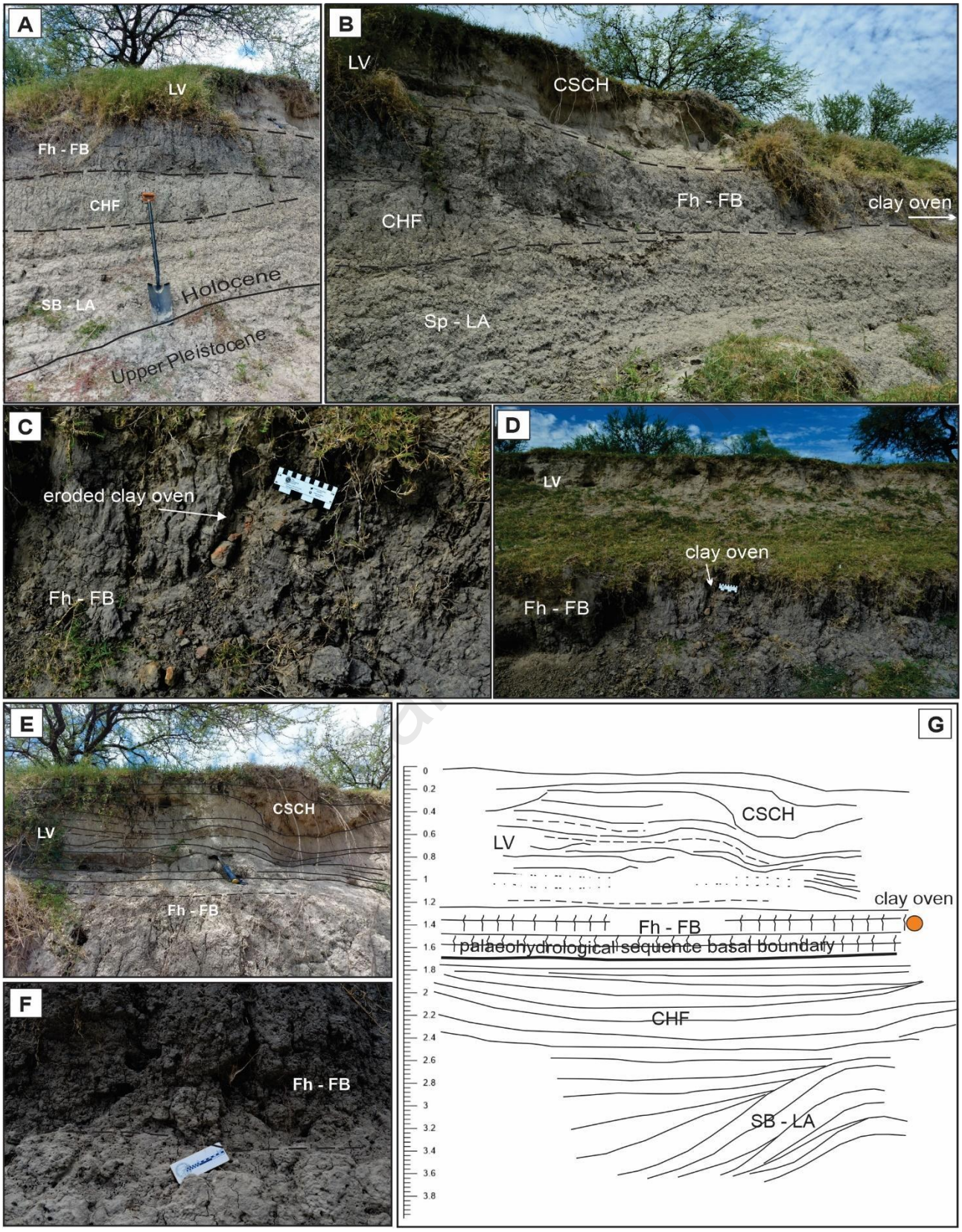

Fig. 5.2- Representative stratigraphic section. The fluvial sequence, interpreted from the vertical association of facies, architectural elements and hierarchy of bounding surfaces, suggests migration of meandering channels (SB-LA), abandonment and fillings of channels (CHF) (see A and B). These were followed by sedimentation from flood cycles and a Bt horizon of a buried soil (Fh-FB (see C, D and F). The Fh-FB architecture constitutes the base of the sequence considered as the palaeohydrological basal boundary. The Late Holocene age of this upper sequence is constrained at the base by the archaeological remain (C and D). The profile of the levee deposits (LV) evidences flood pulses from the grain size and colour of the beds (see

E). The channel forms that cut levee deposits evidence extraordinary floods associated with crevasse-splay sedimentation on the floodplain. G) Interpretative sketch.

3.2. Slackwater indicators in the active floodplain: crevasse splays lobes and crevasse channels

Mid-area of splay lobes. A profile was logged on a cut of an aggradational lobe (31°15'22.30" S, 60°53'59.60"W) into the floodplain (Fig. 6). From bottom to top: brown (7.5YR 5/2) medium sandy bed (0.25 m thick), with few fine Fe-oxide mottles and micas. A fine to medium laminated sandy bed (0.15 m) containing scarce brown (7.5YR 4/3) clayey silt overlies. It is covered by a fine laminated and micaceous sandy bed (0.28 m), light brown (7.5YR 6/3) in colour, with few fine Fe-oxide mottles. The parallel lamination of the sandy beds is horizontal and evolves laterally into an inclined parallel lamination (low angle cross-lamination) (< 10° to the SE). It is capped by a brown (7.5YR 5/2) fine to very fine silty sandy bed (0.27 m), covered by a stratum composed of very fine silty clayey laminated sands (0.25 m), brown (7.5YR 5/2) in colour. Soft sediment deformation caused by loading was observed in the lower layers. Roots and very fine pores are common along the sedimentary profile. Also, buried tree trunks are present. These sandy stratasets that display common medium-scale through cross strata could be interpreted to be formed by dune migration on splay channels, following Bridge (2006). The upward-fining grain size trend evidences abandonment and rapid cessation of discharge, typical of the ephemeral flows in crevasse-splays.

Journal Pre-proof

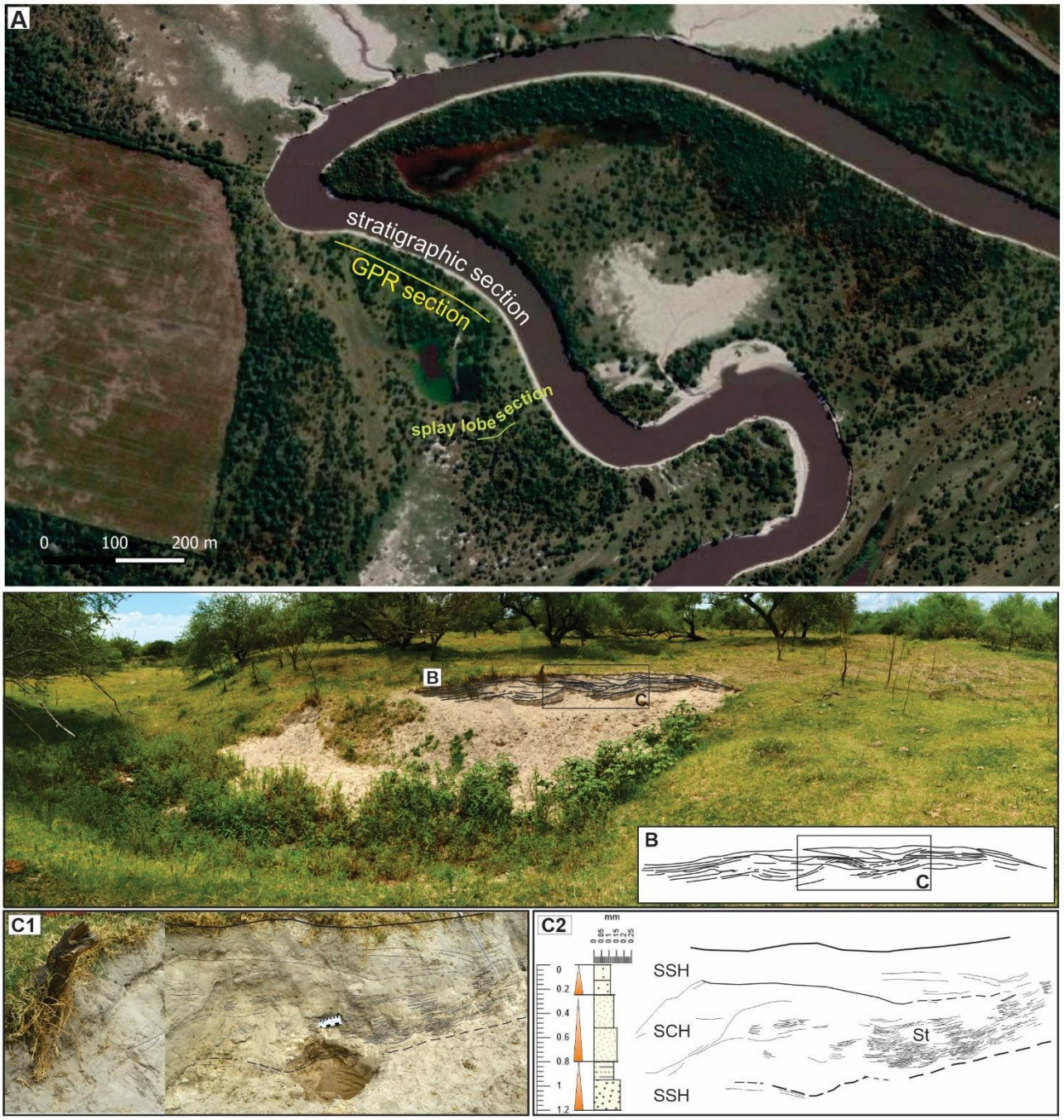

Fig. 6- A) Location of the stratigraphic and GPR cross-sections (Figs. 5.1 and 5.2) and the splay lobe section (6B). 6B) Representative sedimentary section from a splay lobe deposited on the middle area of the splay system. Sand sheets (SSH) and splay channel sands (SCH) accumulated above the horizontal layers of clays sedimented in the floodplain. An upward-fining grain size trend in the strata sets indicates episodic flood cycles.

A borehole into one of the crevasse lobes (Lobe 4; 31°15'20.20"S, 60°54'03.40"W) (Fig. 9) showed the following profile (Fig. 6), from bottom to top: brown (10YR 4/3) sandy clayey bed (0.19 m thick) covered by dark brown (10YR 3/3) clayey fine sandy bed (0.38 m thick). It is interpreted as a floodbasin facies (Bridge, 2006). In transitional contact overlies a stratum (1.44 m thick) composed of very fine to medium sandy beds, light olive-brown (2.5Y 5/4) to very pale brown (10YR 7/3) in colour. Throughout the profile, fine Fe-oxide mottles and micas are common. These sandy strata are interpreted as crevasse-splays.

Journal Pre-proof

Proximal area of splay lobes. A borehole into one of the crevasse lobes (Lobe 3: 31°15'32.30"S, 60°53'47.50" W) (Fig. 7B) was logged near the levee area. From bottom to top: very dark grey (2.5Y 3/1) clayey bed (0.10 m thick) with frequent fine Fe-oxide mottles, which is interpreted as floodbasin facies. It is in clear contact (at 1.55 m deep) with sandy strataset (1.55 m thick), composed of dark olive-brown (2.5Y 3/3) fine silty clayey laminated and micaceous sandy beds interbedded with light yellowish brown (2.5Y 6/3) medium and micaceous sandy beds. Throughout the profile, fine Fe-oxide mottles are common. These sand sheets show upward-fining grain size stratasets. They can be interpreted to be generated by flood episodes from unsteady flows, typical of crevasse-splays.

Distal area of splay lobes. A borehole into the distal area of one of the crevasse lobes (Lobe 2: 31°15'34.40"S, 60°53'47.10" W) (Fig. 7B) was logged. From bottom to top: brown (10YR 4/3) sandy silty clayey bed (0.04 m thick), which is interpreted as a floodbasin facies. It is in clear contact (at 1.17 m depth) with a sand strataset (1.17 m thick). It is composed of pale brown (10YR 6/3) fine to medium sandy beds interbedded with light olive brown (2.5Y 5/3) silty clayey sand. Throughout the profile, fine Fe-oxide mottles and micas are common. These sand sheets of the lobe show an upward-coarsening basal sequence (Fig. 7A) that suggests the progradation of the splay lobe on the adjacent backswamp (Fig. 7B). The upper sequence presents an upward-fining grain size trend, which suggests an abandonment cycle of the splay lobe body.

Journal Pre-proof

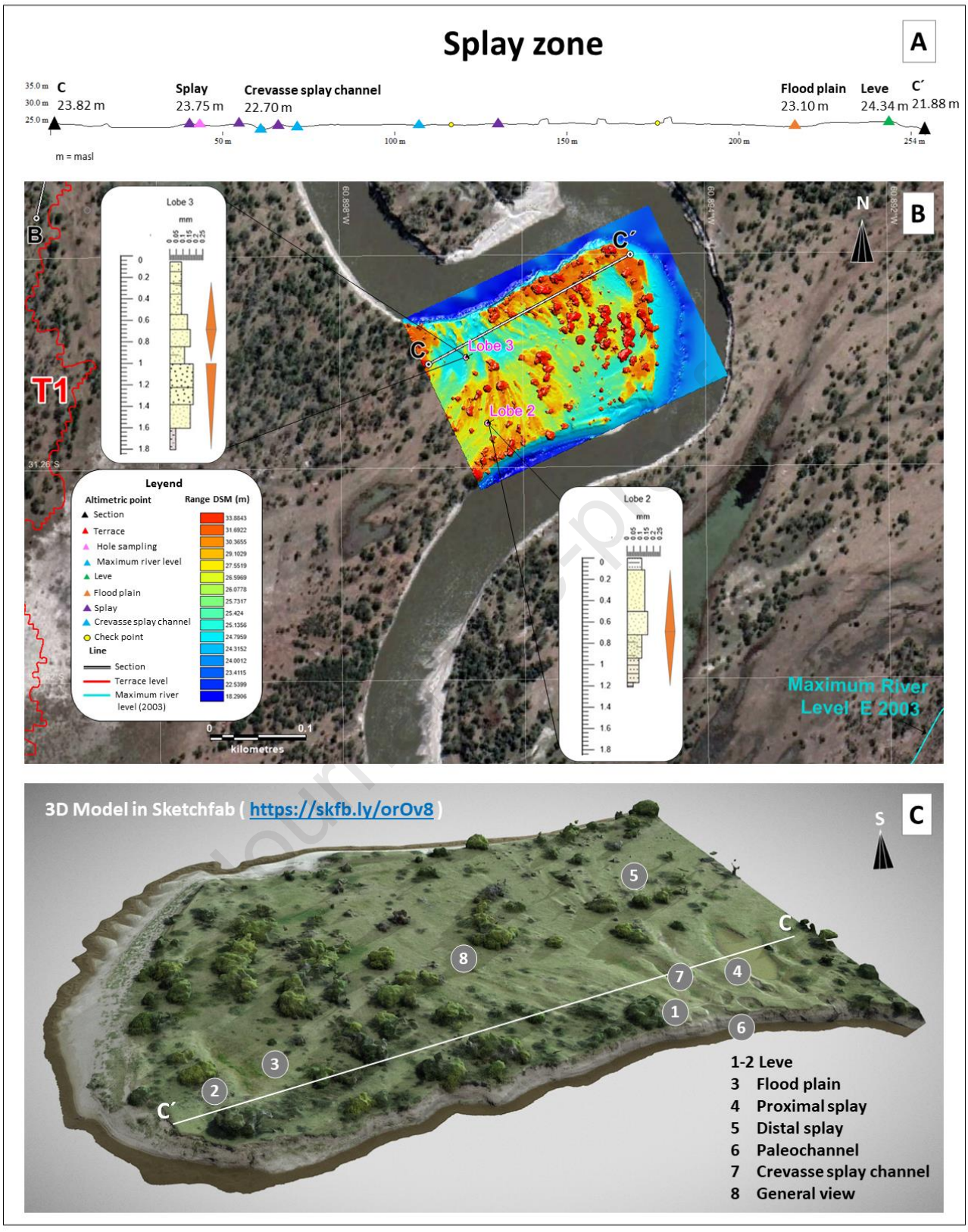

Fig. 7- Model of floodplain landforms from VAN-T optical and DEM high-resolution images. A- Minimum hydrological levels of floods inferred from calibrated geodetic elevations of indicative landforms. B- Sedimentological profiles form boreholes. Profile of lobe 2 shows an upward-coarsening and upward-fining trend, suggesting progradation of lobes and abandonment over flood cycles in the distal area. C- 3D model showing aggradation lobes of splays sedimented upon the floodplain. Forms generated by crevasse-splay channels are evidenced on the erosion bank of the present channel (https://skfb.ly/orOv8).

Journal Pre-proof

3.3. Sedimentological slackwater indicators of the western margin fluvial terraces:

A set of four manual boreholes was performed from a 45 m long cross-section through the highest terrace levels, at the right margin of the fluvial valley (Fig. 8). The profiles show upward-fining sands, ranging from medium sand to silty very fine sand. These sandy beds appear below depths ranging from ca. 1.20 m to 1.65 m (from E to W) (Fig. 8). The deepest coarser grain size bed drilled shows sand better sorted than the rest of the sand. The set of sandy beds was not reached in the westernmost borehole. Overlaying the sandy strata, an upward-fining set of silt beds appears in all of the boreholes. The grain size ranges from sandy silt to clayed silt. The thickness varies from ca. 0.40 m to 0.80 m (from E to W). Particularly, the westernmost borehole displays interbedded very fine sands and silty very fine sands. The suite of sand beds finishes at the top with a sandy silt bed. The upper sandy interbedded stratum is ca. 0.60 m thick. The sequence is covered by clay to clayey silty deposits. These pedogenised mud deposits appear at the top of all of the boreholes. They present a roughly uniform thickness, ranging from 0.70 m to 0.95 m, which suggests a tabular geometry of the sediments near the surface.

The mineralogy of the very fine sand fractions of the drilled sandy beds is represented by subrounded to subangular grains composed of 68% quartz, 20% feldspars (plagioclase, orthoclase and microcline), 5% alterites, 5% heavy minerals (hornblende, diopside, rutile, garnet, monazite, sillimanite, titanite, tourmaline, staurolite, epidote, olivine, and opaque), and 2% micas. These results are similar to the mineralogy observed for Late Holocene sandy strata of sedimentary sequences outcropping along the NSR in the study area (Thalmeier et al., 2021).

Journal Pre-proof

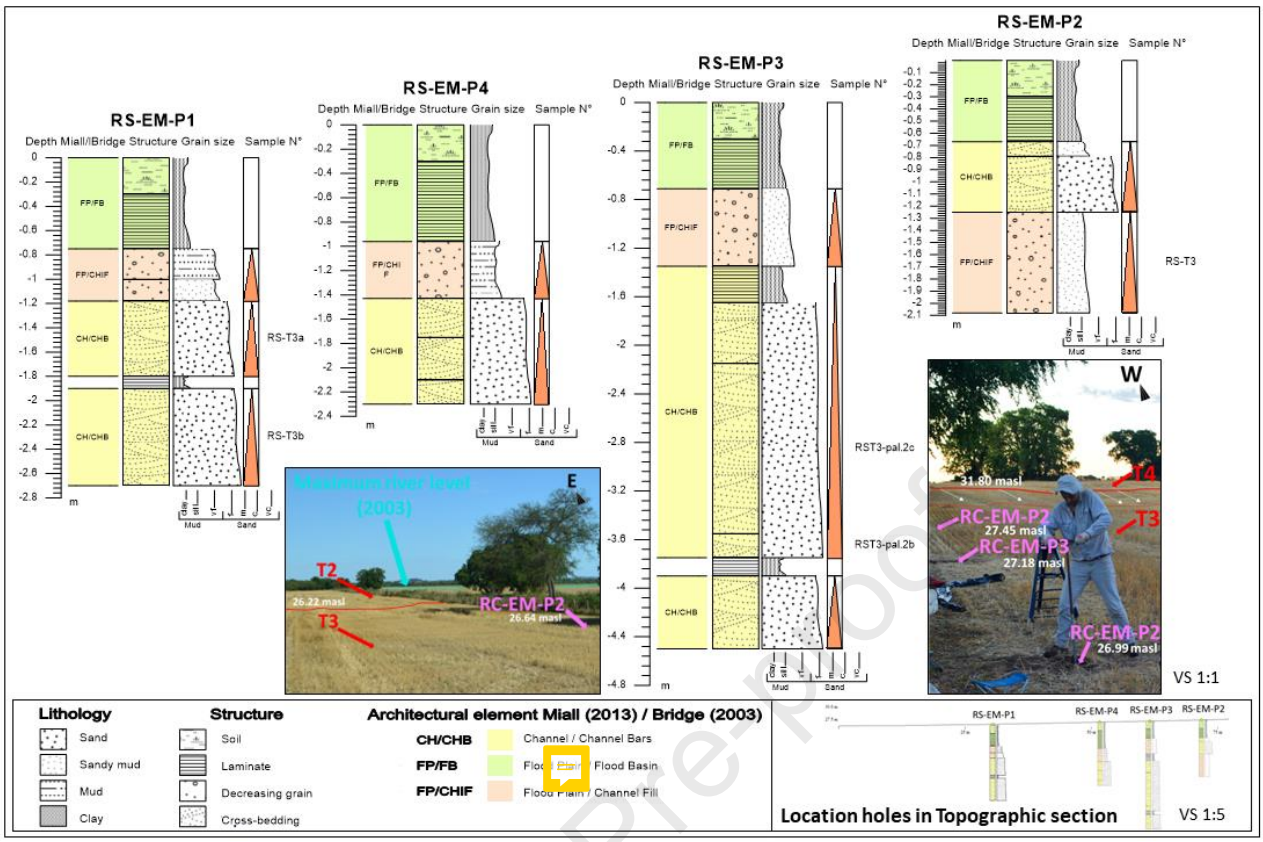

Fig. 8- Borehole sedimentological profiles from the western margin of Late Holocene terraces.

3.4. Geodetic data from UAV Photogrammetry for reconstruction/estimation of hydrological levels

DEMs allowed the extraction of the elevations of the main geomorphological SWIs. These values represent the minimum restored hydrological levels obtained from the preserved sedimentary overbank landforms. They are crevasse splay deposits, levees and fluvial terraces (Fig. 9A) that were logged and checked in natural cuts or from manual boreholes. We identified levels comparable with altitudes of the maximum flood line recorded in the yr. 2003 peak event. This 2003 flood line is roughly comparable with the subtle riser between the labelled T1 and T2 terraces (Fig. 9A). The well-preserved staircase of terrace T2 and the relict of terrace T3, stranded on the valley side (Fig. 9A), correspond to levels up to 7-9 m above the present main channel and ca 2.5-3 m above the maximum level reached over the 2003 flood. From the HD DEM, we registered an elevation of 24.37 masl. for the maximum 2003 flood line through the belt of the cross-section obtained from the drone (Fig 9C). T1 terrace surface elevations range between 23.77 and 24.15 masl. T2 appears at 24.30 and 26.22 m ASL, while the narrow relic of the T3 surface appears between 26.22 and 28.0 masl.

It is noteworthy that the well-preserved fluvial levee, located adjacently to the present main channel of the NSR, displays an elevation of 26.66 m asl in a checking point (Fig. 9C). In the logged section (Fig. 9B) the maximum elevation is slightly lesser than 25 masl. Considering the calculated precision of the obtained geodetic data, it is not possible to be conclusive. However, the levee located on the left margin of the present main channel seems not to have been exceeded by the yr. 2003 flood (24.37 masl). Optical satellite images recording this extreme event suggest that it is true, although image resolution is poor. Crevasse splays,

surveyed by drone and checked in the field, appear to have been sedimented under flood levels slightly lesser than the maximum yr. 2003 flood water level (Fig. 9). We register altitudes of 24.15 masl in these crevasse splays. This elevation is comparable to the T1-T2 boundary, and it is very close to the maximum water level of the yr. 2003 flood (Fig. 9C).

Journal Pre-proof

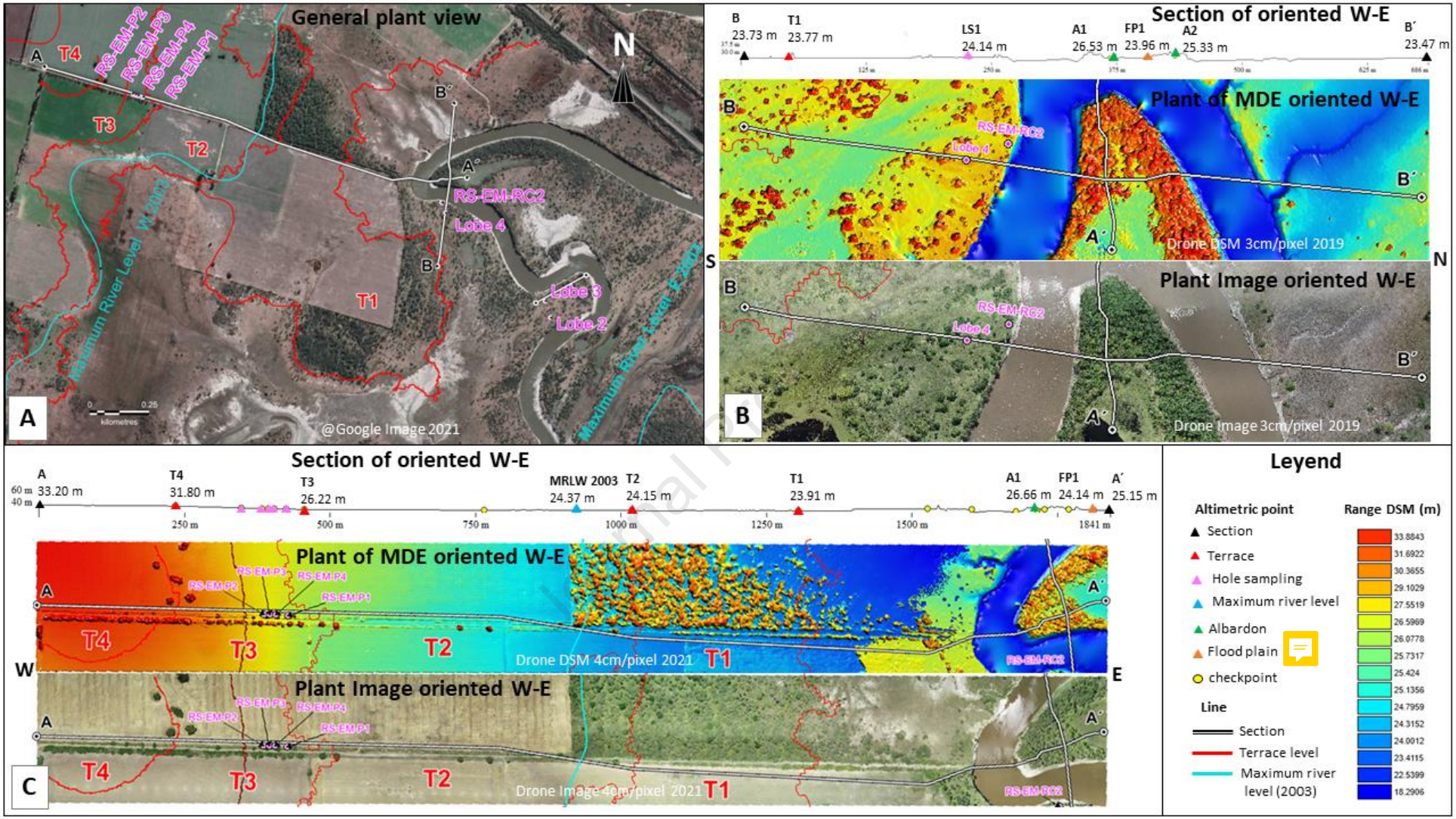

Fig. 9 – Geodetic hydrological levels rebuilt from a high-resolution swath cross-section of the current active floodplain and channel, obtained from the drone survey. Estimated elevations of terraces and floodplain landforms (fluvial levees and splays) allow us to infer flood levels above the historical extreme episodes of years 1914 and 2003.

3.5. GPR stratigraphic analyses

We interpreted the subsurface fluvial architecture of the NSR by analysing a cross-section L42 radargram (Fig. 10). The most superficial GPR reflectors of the section cross transversely the higher terrace level and the edge of the Holocene fluvial valley. Based on the correlation of analogous fluvial architectural elements in outcrop profiles with GPR data, the internal elements are interpreted as follows (adapted from (Bridge, 2006; Miall, 2013)):

Floodplain/Floodbasin architectural element (FP/FB). The internal reflections appear as semi-continuous wavy divergent oblique fill. There is internal convergence at the slope break, and reflection spacing expands and onlaps the adjacent elements.

Bounding Surfaces: within the element, bounding surfaces are difficult to distinguish. The upper and lower bounding surfaces are minor laterally continuous dipping reflections except for the CH included in this unit.

Channel fill architectural element (CHF). Internal reflections show a variety of fill patterns including onlapping, divergent, prograding, and complex fillings.

Bounding Surfaces: Strong lower bounding surface creates concave-up well-developed reflections. They show near-horizontal to little or no difference between bounding shallow dipping parallel geometries.

Channel Bars architectural element (CH/CHB). Reflections show well-developed, near-horizontal to little or no difference between bounding shallow dipping parallel geometries.

Bounding Surfaces: Little or no difference between bounding reflections; therefore, bounding surfaces are inferred from the change in the reflection patterns. Reflection present parallel sigmoid with well-developed, laterally continuous geometries.

Bounding surfaces are oriented similarly to internal surfaces. Boundaries are marked by changes in reflection patterns. Adjacent elements may be conformable or may show truncation of lower reflections.

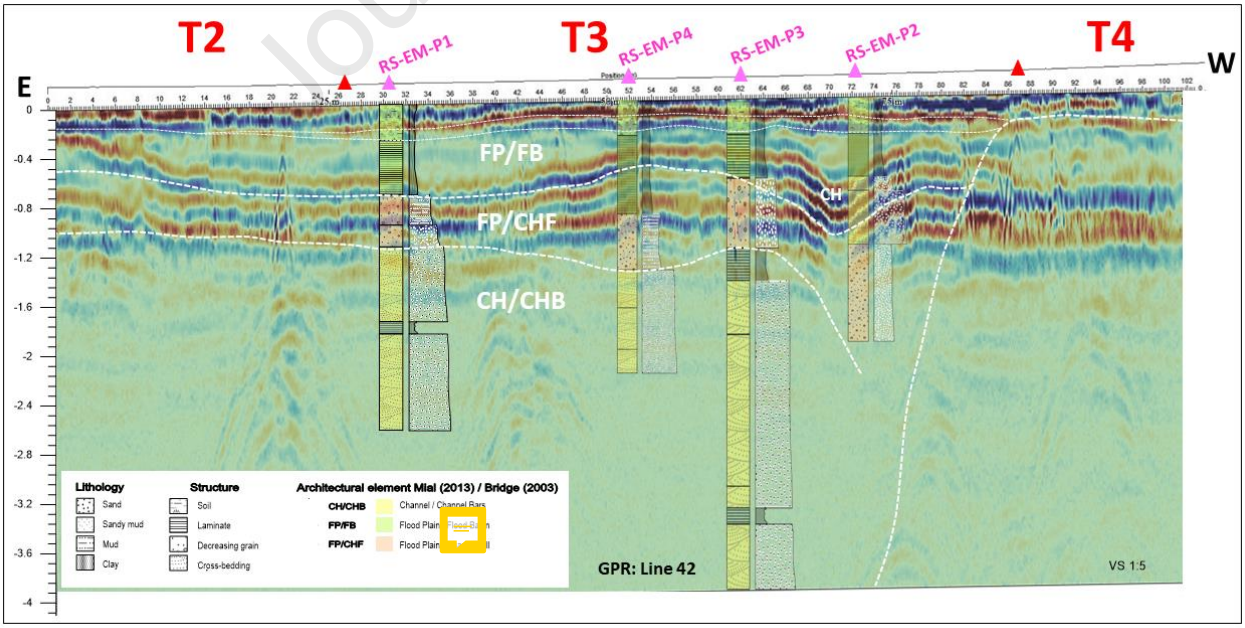

Fig. 10. Sequence fluvial stratigraphy from the GPR section. Vertical elevations were calibrated from high-resolution DEM generated from the drone. The interpretation was supported by the sedimentology from the in-situ boreholes and the stratigraphy analysed on outcrops in the erosion banks of the main channel (Figs. 5.1 and 5.2). The fluvial sediments are interpreted as deposits that were sedimented on the western valley margin

of the active system. The uppermost sequence of beds is associated with different terrace levels and with extreme flood stages (T2; T3 and T4, see Figs. 9 and 11).

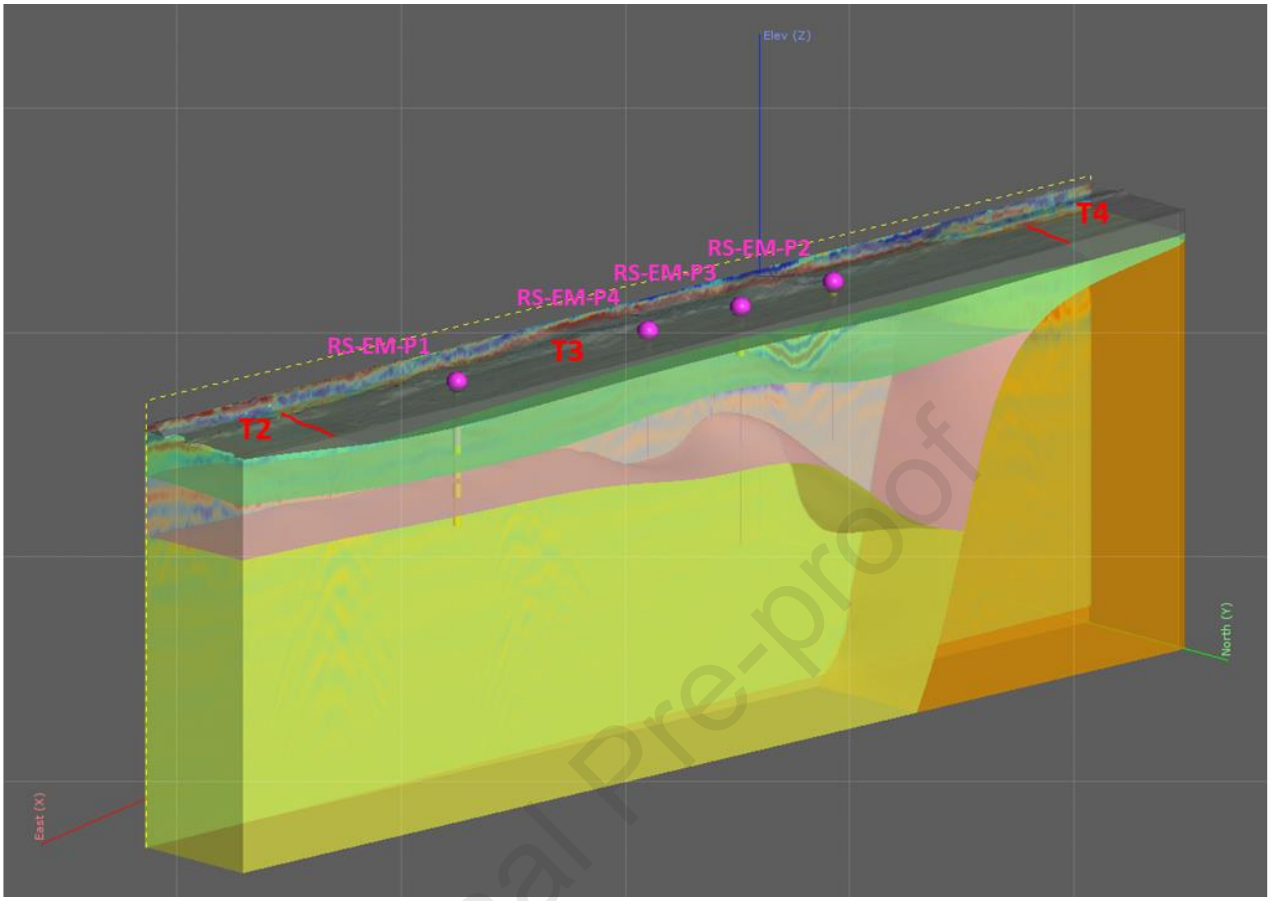

Fig. 11- Implicit modelling from Leapfrog Geo. 3D representation of the integrated multi-proxy data reproducing flooding indicators, in the western margin of the NSR in the Manucho area.

3.6. Hydrological record

The previously calculated hydrogram for the episode of May 2003 (MAH-UNL, 2006) allowed their authors to estimate a peak discharge of 3403 m^3/s for the NSR. If we apply the proposed equation for the altitude-discharge curve for this hydraulic section, we can infer simulated discharge values for the water levels of the SWI-PSI identified in the field. From the geodetic data of the highest Holocene terrace and fluvial levee altitudes above the water level reached at the yr. 2003 flood peak, discharges ranging from 5109 to 6257.2 m^3/s can be inferred (Table 3). These estimations would represent peak discharge values 50-80% higher than those of the yr. 2003 flood (Table 3).

Flood indicator	Elevation (m.a.s.l.)	Local hydrometric level (m)	Discharge (m^3/s)	Estimated discharge excess (%)
yr. 2003 flood peak	24,37	13,28	3449	0,0
T1 top	24,3	13,21	3386	-1,8
T2 top	26,22	15,13	5109	48,1
T3 top	27,5	16,41	6257	81,4
Levee	26,66	15,57	5503	59,6

Table 3 – Simulated discharges for extreme flood indicators

3.7. Hydrological record. 1914 flood event

Research carried out by hydrologists produced a reconstruction of absolute elevations of flood marks attributed to the yrs. 1913-1914 flood of the NSR. These marks were recognised and estimated from documents, maps and photographs, and restored from measurements in the field (Gardiol and Ocampo, 2017). The study reported a restored yr. 1914 flood peak water level of 22.64, 22.68, and 23.45 masl according to the different methodologies applied. The estimated values correspond to Paso Vinal, a point on the NSR fluvial valley, 16 km downstream from the Manucho study area. These values plotted in our processed DEMs show a good correlation with the yr. 2003 peak flood line from satellite images. This observation reinforces the hypothesis that both extreme events were similar in discharge magnitude and hydrological characteristics. The authors obtained a range of discharges for the yr. 1914 event from hydrological modelling, comparable with values of discharges estimated for the yr. 2003 event.

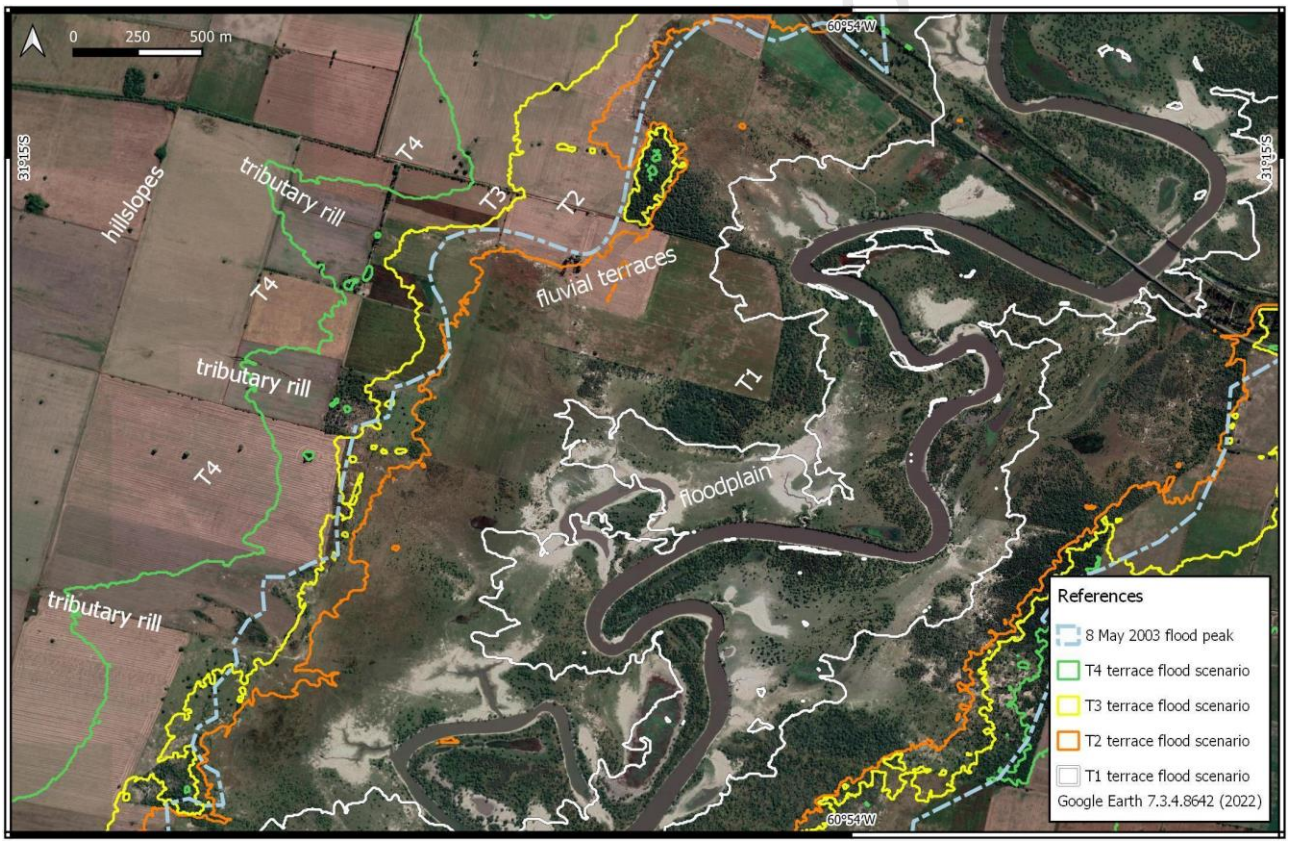

Fig. 12 – Map of flood-prone areas from different proxies. Different flood scenarios were constructed from low-lying areas routine, calibrated by the automated method of extraction of terrace surfaces (Fig. 3). T2 and T3 flood scenarios overcome the maximum instrumentally recorded yr. 2003 event. The flood occurred in 1914 was estimated to be equivalent in magnitude to that of the yr. 2003 episode.

Discussion

A multi-proxy approach that integrates fluvial sedimentological and stratigraphic data, GPR subsurface sections and calibrated geodetic data from UAV photogrammetry allowed us to reconstruct hydrological levels

of large palaeofloods. This integral methodology was based on the recognition of the widely-applied SWI-PSIs (Baker, 2008; Benito et al., 2020; Benito and Hudson, 2010; Gregory et al., 2006).

The geomorphic mapping shows the spatial distribution of fluvial landforms that indicate areas affected by floods (Fig. 2). They can be discriminated as landforms of the active floodplain and terraces (Fig. 3).

It is assumed that the SWI or flood deposits of the terraces must be associated with the modern flood regime of the river. Moreover, the cross-sections of the channels have to remain relatively stable (Benito and Hudson, 2010). In that way, 2D and 3D architectural analysis of Holocene fluvial sedimentological bodies can provide a frame for the palaeohydrological observations. Long-term sequence analysis at the Holocene time-scale would allow us to discriminate and constrain the record of the "active" dynamics involving potential extreme events associated with climate changes or long-term maximum events. Therefore, the sequence stratigraphic model described in the field (Figs. 5.1 and 5.2) shows that the upper cycle characterised by vertical accretion of sediments can be considered as the long-term "active" system. Fine deposits of the floodplain appear on the top of the younger terraces. The discovery of archaeological remains at the base of this upper floodplain sequence supports a centennial to millennial age-scale lesser than 2.5 ka BP. Roldán and Kröhling (2021) deduced from regional geoarchaeological and stratigraphic analyses two levels of human occupation in the lower Salado River Basin over the Holocene. They used buried baked clay ovens as a spatial and temporal marker. The ovens were built by the Esperanza Culture (Ceruti, 2019). The oldest level of occupation is ca. 2.5 ka. BP (Cornero et al., 2013) and the youngest one, ca. 1 ka. BP (Medieval Warm Period -MWP) (Cornero et al., 2013; Del Río et al., 2016; Del Río and Cornero, 2017). They are located mainly on Holocene fluvial landforms (e.g. crevasse splays and fluvial levees). A partially eroded clay oven was found in the upper part of the Bt horizon of the palaeosol identified in the studied profile (Fig. 5.2.). It is buried beneath the recent levee deposits. Based on the findings in the near region, we might infer an age in the range of 1-2.5 ka.

The edges of the fluvial valley are good places to examine the most extreme palaeoflood record. Terraces whose elevations are above the historical (yr. 1914) and recent maximum flood level (yr. 2003) are the best clues. GPR subsurface data show that these surfaces form part of the fluvial dominium. Channels covered by horizontal floodplain geometries are detected from radargrams. Furthermore, these horizontal beds show a terraced geometry (Fig. 9), which suggests the occurrence of different flood stages. Grain-size and mineralogic descriptions of samples from manual boreholes confirm the sequence interpretation from GPR images. Considering subsurface information and field observations, we can state that the T4 level (Late Pleistocene deposits) is the non-exceedance discharge threshold for the palaeohydrological record of the area. This is a stable terrace not linked with the current fluvial dynamics.

In the current floodplain, other flood diagnostic landforms situated near the main channel are useful to evidence discharges unprecedented for the instrumental record. Fluvial levee deposits present elevations above the restored value of the maximum elevation for the May 2003 flood peak in the Manucho area (MAH-UNL, 2006). This recent episode resulted to be catastrophic for a big city like Santa Fe, located 60 km downstream. However, geodetic data from the reported flood diagnostic landforms suggest that the NSR system is able to produce episodes even worse.

We demonstrated here that terrace T1 may be affected in a flood episode similar to the yr. 2003 flood occurred in Manucho. The comparison with the reconstruction of hydrological level of the yr. 1914 event (Paso Vinar) suggests that T1 (altitudes ranging from 23.77 to24.30 m) represents a geomorphological equilibrium stage for extreme events, such as the ones recorded in yrs. 1914 and 2003. The altitude measured on the top of splay lobes (24.15 m) suggests that these episodes correspond with these events or similar ones in magnitude. This implied an adjustment of the fluvial landscape to define abandonment of this unit in normal flood events, which affected the current floodplain. Present land-use proves that inference (Fig. 11). However, T2 (24.30 - 26.22 m), top of the levee (26.66 m) and T3 (26.22-28.00 m) appears as geomorphological indicators of higher stages. An intensive plan of geochronological data collection from the identified fluvial sediments would help to build a long-term recurrence curve based on physical evidence. This could reinforce recurrence estimations of extraordinary NSR floods, usually extrapolated from the instrumental record (e.g. Paoli et al., 2015). In that case, the fitting would be based on physical data. In addition, high-resolution geochronological data collected from the cyclical bedded deposits in levees would enable us to build intermediate terms of the recurrence interval. Several pulses of floods are well-defined from upward-fining sedimentary cycles in the levee deposits observed in the Manucho area (Fig. 5.2).

Moreover, if a dynamic equilibrium is assumed and predictions of intensification of extreme events are confirmed, these extreme floods could become more frequent. It has been widely reported that the large rivers of the Rio de la Plata basin have increased medium discharges from yr. 1970 as well as extreme discharges (Barros et al., 2015). A positive trend of annual rainfall has also been observed over the last 50 years in the Paraná - Río de la Plata lower basin (Doyle and Barros; Barros et al., 2013). Rainfall intensity indices show that short-time extreme events are more frequent in the region (Calcavanti et al, 2015), and widen the amplitude of wet and dry peaks over the last decades (Lovino et al., 2022). The severe episodes are characterised by heavier rainfalls with larger magnitude and intensity (Calcavanti, et al. 2015). All models predicting different scenarios project the persistence of this trend in the Paraná and Uruguay river basins (Barros et al., 2013; 2015).

In this context, geomorphometric techniques appear to be robust tools for predicting potential scenarios. In absence of the possibility of applying complex hydrological “direct” models that require input data difficult to access, geomorphometric procedures are straightforward and efficient methods to attain useful results (Baker, 2008; Benito and Hudson 2008). Automated methods for the extraction of terrace surfaces from DEMs (Demoulin et al., 2007; Józsa, 2019) or by means of the map algebra computation applied in this work result suitable to map areas prone to flooding. The intersection of terrace mapping with “simulation of low-flat areas” as a procedure to reproduce flooding scenarios can offer reliable results when they are calibrated from geomorphological and sedimentological data (Fig. 12). This is the classical reasoning based on inverse modelling applied to geology. The geomatic method for the extraction of terrace elevations and field control supplies valuable elements to estimate discharges in extreme flooding scenarios (Fig.12).

The discharge values from SWI-PSIs projected here, 50-80% higher than the maximum discharges instrumentally estimated, indicates that it is necessary to assess carefully flood hazards in the lower basin of the NSR. The geological perspective appears to be broader than the classical hydrological approach, based on

short-term frequency analyses. A long-term perspective that integrates multi-proxy data would help to avoid underestimating flood hazards related to extreme weather events in the present context of fast climate change. We cannot disregard the fact that higher terraces might represent analogues of new adjustments in the fluvial geomorphology for the near future. They would represent palaeostages as flood responses to climate variability (Ely, 1993; Knox 2000). That consideration means that we should not only expect low-frequency large events but also to project higher energy flows as a medium stage.

Conclusions

A representative segment of the Northern Salado River (NSR) (Manucho site), a typical meandering river of flat plains in South America, is a study case useful for the identification of SWI-PSIs. Fluvial landforms associated with floods seem to be reliable indicators of large floods in this sensitive system. Sedimentological and geomorphic indicators evidenced the occurrence of floods larger than the maximum extreme events recorded from historical information (yr. 1914 flood peak) and the recent yr. 2003 flood peak, instrumentally recorded.

The proposed convergent geomorphometric routines, based on calibrated DEM information (extraction of discrete terrace surfaces, automated geomorphones and low-lying areas estimations) proved to be an efficient methodology for mapping flood-prone areas over extreme episodes. These areas exceed areas flooded over yr. 2003 peak in the Manucho site.

Stratigraphy and shallow geophysics research in fluvial environments enable us to define the palaeohydrological non-exceedance discharge thresholds. The dating of sedimentary cycles observed in the analysed SWI-PSIs and the estimations of discharges from geodetic data associated with these overbank landforms could provide valuable information for building flood recurrence curves based on physical information. That would be primarily useful in regions characterised by short-time series of hydro-climatic data, such as the studied area. The archaeological finding at the base of flood deposits indicate maximum ages ca. 2.5 ka for the analysed SWI-PSI in the NSR.

The estimates of discharges for these extreme palaeofloods, reproducing potential scenarios in NSR, show values 50-80% higher than discharges calculated for the yr. 2003 maximum event instrumentally recorded. According to this information, it is essential to address quantitative fluvial geomorphological studies in basins that deliver water to large rivers of plains, such as the Paraná river, as they are extremely sensitive to large floods.

This perspective should be considered in territory planning and management. Considering this hazard magnitude, further studies to assess flood vulnerability in Santa Fe city should be conducted.

Acknowledgements

Fieldworks were funded by Project IO-2019-183 (coordinated by Dr P. Cello and D. Kröhling) from ASaCTei (Agencia Santafesina de Ciencia, Tecnología e Innovación) and by Project 50620190100127LI CAI+D 2020

PI TIPO II (coordinated by D. Kröhling) from the UNL (Universidad Nacional del Litoral), Santa Fe, Argentina. This work was also supported by Seequent providing a License for Leapfrog GeoTM for the research to the Laboratory of Plain Geology (LAGEO-CICyTTP-CONICET-UADER). Many thanks to English reviser M. Herman, which work was funded by the PRODACT-FICH-UNL grant. We are very grateful to VSI Rivers and Wetlands special volume editors and reviewers for their thoughtful comments and recommendations, which have improved the manuscript.

References

Allen, J.R.L., 1983. Studies in fluviatile sedimentation: bars, bar-complexes and sandstone sheets (low-sinuosity braided streams) in the Brownstones (L. Devonian). Welsh Borders. Sediment. Geol. 33, 237–293.

Baker, V.R., 2013. Global Late Quaternary Fluvial Paleohydrology: With Special Emphasis on Paleofloods and Megafloods, in: Treatise on Geomorphology. Elsevier Inc., pp. 511–527. https://doi.org/10.1016/B978-0-12-374739-6.00252-9

Baker, V.R., 2008. Paleoflood hydrology: Origin, progress, prospects. Geomorphology 101, 1–13. https://doi.org/10.1016/j.geomorph.2008.05.016

Barros, V.R., Boninsegna, J.A., Camilloni, I.A., Chidiak, M., Magrín, G.O., Rusticucci, M., 2015. Climate change in Argentina: Trends, projections, impacts and adaptation. Wiley Interdiscip. Rev. Clim. Chang. 6, 151–169. https://doi.org/10.1002/wcc.316

Benito, G., Harden, T.M., O'Connor, J., 2020. Quantitative Paleoflood Hydrology. Treatise Geomorphol. 743–764. https://doi.org/10.1016/b978-0-12-409548-9.12495-9

Benito, G., Hudson, P.F., 2010. Flood hazards: The context of fluvial geomorphology, in: Geomorphological Hazards and Disaster Prevention. Cambridge University Press, pp. 111–128. https://doi.org/10.1017/CBO9780511807527.010

Benito, G., O'Connor, J.E., 2013. Quantitative Paleoflood Hydrology, Treatise on Geomorphology. Elsevier Ltd. https://doi.org/10.1016/B978-0-12-374739-6.00250-5

Bodoque, J.M., Díez-Herrero, A., Eguibar, M.A., Benito, G., Ruiz-Villanueva, V., Ballesteros-Cánovas, J.A., 2015. Challenges in paleoflood hydrology applied to risk analysis in mountainous watersheds - A review. J. Hydrol. 529, 449–467. https://doi.org/10.1016/j.jhydrol.2014.12.004

Bridge, J.S., 2006. Fluvial Facies Models: Recent Developments, in: Facies Models Revisited. SEPM (Society for Sedimentary Geology), pp. 85–170. https://doi.org/10.2110/PEC.06.84.0085

Bridges, R.A., Castle, J.W., 2003. Local and regional tectonic control on sedimentology and stratigraphy in a strike-slip basin: Miocene Temblor Formation of the Coalinga area, California, USA. Sediment. Geol. 158, 271–297. https://doi.org/10.1016/S0037-0738(02)00314-7

Bristow, C., Pugh, J., Goodall, T., 1996. Internal structure of aeolian dunes in Abu Dhabi determined using ground-penetrating radar. Sedimentology 43, 995–1003. https://doi.org/10.1111/j.1365-3091.1996.tb01515.x

Bristow, C.S., Neil Chroston, P., Bailey, S.D., 2000. The structure and development of foredunes on a locally prograding coast: Insights from ground-penetrating radar surveys, Norfolk, UK. Sedimentology 47, 923–944. https://doi.org/10.1046/j.1365-3091.2000.00330.x

Brovkin, V., Brook, E., Williams, J.W., Bathiany, S., Lenton, T.M., Barton, M., DeConto, R.M., Donges, J.F., Ganopolski, A., McManus, J., Praetorius, S., de Vernal, A., Abe-Ouchi, A., Cheng, H., Claussen, M., Crucifix, M., Gallopín, G., Iglesias, V., Kaufman, D.S., Kleinen, T., Lambert, F., van der Leeuw, S., Liddy, H., Loutre, M.F., McGee, D., Rehfeld, K., Rhodes, R., Seddon, A.W.R., Trauth, M.H., Vanderveken, L., Yu, Z., 2021. Past abrupt changes, tipping points and cascading impacts in the Earth system. Nat. Geosci. 2021 148 14, 550–558. https://doi.org/10.1038/s41561-021-00790-5

Brunetto, E., Kröhling, D.M., Zalazar, M.C., Francisconi, M.C., 2017. Analysis of the interaction between neotectonic and surface processes in a low-land intracratonic setting of South America. Quat. Int. 438, 141–159. https://doi.org/10.1016/j.quaint.2016.06.018

Brunetto, E., Sobrero, F.S., Gimenez, M.E., 2019. Quaternary deformation and stress field in the Río de la Plata Craton (Southeastern South America). J. South Am. Earth Sci. 91, 332–351. https://doi.org/10.1016/j.jsames.2017.04.010

Cafaro, E., Latrubesse, E., Ramonell, C., Montagnini, M.D., 2009. Channel pattern arrangement along Quaternary fans and mega-fans of the Chaco plain, central South America, in: Vionnet, C., Garcia, M., Latrubesse, E., Perillo, G. (Eds.), RCEM 2009 River Coastal and Estuarine Morphodynamics. Vols. 1 and 2. CRC Press-Taylor Francis Group, Netherlands. pp. 349–354.

Catt, J.A., Rutter, N., Catto, N.R., 1990. Paleopedology Manual, Paleopedology Manual, Catt J. A. (Ed.), Quaternary International, 6:1-95. INQUA/Pergamon Pres.

Cavalcanti, I.F.A., Carril, A.F., Penalba, O.C., Grimm, A.M., Menéndez, C.G., Sanchez, E., Cherchi, A., Sörensson, A., Robledo, F., Rivera, J., Pántano, V., Bettolli, L.M., Zaninelli, P., Zamboni, L., Tedeschi, R.G., Dominguez, M., Ruscica, R., Flach, R., 2015. Precipitation extremes over La Plata Basin - Review and new results from observations and climate simulations. J. Hydrol. 523, 211–230. https://doi.org/10.1016/j.jhydrol.2015.01.028

Ceruti, C., 2019. Despojados de la tierra indígenas del Paraná-Plata., in: Historia de Santa Fe. ATE, Santa Fe, pp. 21–44.

Cornero, S., Del Río, P., Ceruti, C., 2013. Sitios con hornitos del Holoceno tardío en el chaco austral: Colonia Dolores, dpto. San Justo, pcia. Santa Fe. Anu. Arqueol. Rosario 5, 103–115.

Collinson, J.D., 1996. Alluvial sediments., in: Reading, H.G., Ed.,Sedimentary Environments: Processes, Facies, and Stratigraphy. Blackwell Science, Oxford, pp. 37–81.

Del Río, P., Cornero, S., 2017. Laguna La Blanca: Abordaje espacial en un sitio del holoceno tardío. La Criolla, San Justo, Provincia de Santa Fe. Divulg. la Prod. Científica y Tecnológica la UNR. 571–578.

Del Río, P., Cornero, S., Ceruti, C.N., Echegoy, C., 2016. Arqueología de los Bajos Submeridionales: sitios con hornos de tierra cocida en la localidad arqueológica Laguna La Blanca (La Criolla, Departamento San Justo, provincia de Santa Fe). Rev. Antropol. del Mus. Entre Ríos 2, 68–83.

del Val, M., Iriarte, E., Arriolabengoa, M., Aranburu, A., 2015. An automated method to extract fluvial terraces

from LIDAR based high resolution Digital Elevation Models: The Oiartzun valley, a case study in the Cantabrian Margin. Quat. Int. 364, 35–43. https://doi.org/10.1016/j.quaint.2014.10.030

Demoulin, A., Bovy, B., Rixhon, G., Cornet, Y., 2007. An automated method to extract fluvial terraces from digital elevation models: The Vesdre valley, a case study in eastern Belgium. Geomorphology 91, 51–64. https://doi.org/10.1016/j.geomorph.2007.01.020

Ferrero, M.E., Villalba, R., 2019. Interannual and Long-Term Precipitation Variability Along the Subtropical Mountains and Adjacent Chaco (22-29° S) in Argentina. Front. Earth Sci 7, 148. https://doi.org/10.3389/feart.2019.00148

Forlani, G., Diotri, F., di Cella, U.M., Roncella, R., 2019. Indirect UAV strip georeferencing by on-board GNSS data under poor satellite coverage. Remote Sens. 11. https://doi.org/10.3390/rs11151765

Gabrlik, P., Jelinek, A., Janata, P., 2016. Precise Multi-Sensor Georeferencing System for Micro UAVs. IFAC-PapersOnLine 49, 170–175. https://doi.org/10.1016/j.ifacol.2016.12.029

Gardiol, M., Ocampo, C.J., 2017. Reconstrucción de niveles máximos de la crecida de 1913-1914, in: Gardiol, M.R., Morresi, M. del V. (Eds.), Rio Salado: Un Aporte Al Conocimiento de La Crecida Extraordinaria de 1914. Universidad Nacional del Litoral, Santa Fe, pp. 81–132.

Garreaud, R.D., Vuille, M., Compagnucci, R., Marengo, J., 2009. Present-day South American climate. Palaeogeogr. Palaeoclimatol. Palaeoecol. 281, 180–195. https://doi.org/10.1016/j.palaeo.2007.10.032

GRASS Development Team, 2022. Geographic Resources Analysis Support System (GRASS) Software, Version 8.0. Open Source Geospatial Foundation. https://grass.osgeo.org.

Gregory, K.J., Benito, G., Dikau, R., Golosov, V., Johnstone, E.C., Jones, J.A.A., Macklin, M.G., Parsons, A.J., Passmore, D.G., Poesen, J., Soja, R., Starkel, L., Thorndycraft, V.R., Walling, D.E., 2006. Past hydrological events and global change. Hydrol. Process. https://doi.org/10.1002/hyp.6105

Horton, B.K., DeCelles, P.G., 2001. Modern and ancient fluvial megafans in the foreland basin system of the central Andes, southern Bolivia. Basin Res. 13, 43–63.

Instituto Geográfico Nacional. Dirección de Geodesia, 2017. Red de Nivelación de la República Argentina. http://ramsac.ign.gob.ar/posgar07_pg_web/documentos/Informe_Red_de_Nivelacion_de_la_Republica_Argentina.pdf.

Instituto Geográfico Nacional, 2021. Modelo Digital de Elevaciones de la República Argentina versión 2.1.

Iriondo, M., 1993. Geomorphology and late Quaternary of the Chaco (South America). Geomorphology 7, 289–303. https://doi.org/10.1016/0169-555X(93)90059-B

Jasiewicz, J., Stepinski, T.F., 2013. Geomorphons-a pattern recognition approach to classification and mapping of landforms. Geomorphology 182, 147–156. https://doi.org/10.1016/j.geomorph.2012.11.005

Jiménez Cisneros, B.E., Oki, T., Arnell, N.W., Benito, G., Cogley, J.G., Döll, P., Jiang, T., Mwakalila, S.S., 2014. Freshwater resources, in: Field, C.B., Barros, V.R., Dokken, D.J., Mach, K.J., Mastrandrea, M.D., Bilir, T.E., Chatterjee, M., Ebi, K.L., Estrada, Y.O., Genova, R.C., Girma, B., Kissel, E.S., Levy, A.N., MacCracken, S., Mastrandrea, P.R., White, L.L. (Eds.), Climate Change 2014: Impacts, Adaptation, and Vulnerability. Part A: Global and Sectoral Aspects. Contribution of Working Group II to the Fifth Assessment Report of the Intergovernmental Panel on Climate Change. Cambridge University Press,

Cambridge / Nueva York, pp. 229–269. https://doi.org/10.1017/CBO9781107415379.008

Józsa, E., 2019. Geomorphometric application of quasi-global DEMs for semi-automated geomorphological mapping. University of Pécs. http://pea.lib.pte.hu/handle/pea/23445.

Knox, J.C., 2000. Sensitivity of modern and Holocene floods to climate change, Quaternary Science Reviews.

Kochel, R.C., Baker, V.R., 1988. Paleoflood analysis using slackwater deposits. J. Environ. Sci. English Ed. 357–376.

Kruck, W., Helms, F., Geyh, M.A., Suriano, J.M., Marengo, H.G., Pereyra, F., 2011. Late Pleistocene-Holocene History of Chaco-Pampa Sediments in Argentina and Paraguay. E&G Quat. Sci. J. 60, 188–202. https://doi.org/10.3285/eg.60.1.13

Lastra, J.A.S., López Carmona, M., López Mendoza, S., 2008. Tendencias del cambio climático global y los eventos extremos asociados. Ra Ximhai Rev. científica Soc. Cult. y Desarro. Sosten. 4, 625–633.

Latrubesse, E.M., 2003. The Late Quaternary Paleohydrology of Large South American Fluvial Systems. Palaeohydrology Underst. Glob. Chang. 193–213.

Leigh, D.S., 2018. Vertical accretion sand proxies of gaged floods along the upper Little Tennessee River, Blue Ridge Mountains, USA. Sediment. Geol. 364, 342–350. https://doi.org/10.1016/j.sedgeo.2017.09.007

Leopold, L.B., Wolman, M.G., Miller, J.P., 1964. Fluvial processes in geomorphology. New York W.H. Free. Co. 522.

Lovino, M.A., Müller, G. V., Pierrestegui, M.J., Espinosa, E., Rodríguez, L., 2022. Extreme precipitation events in the Austral Chaco region of Argentina. Int. J. Climatol. 1–22. https://doi.org/10.1002/JOC.7572

Ministerio de Asuntos Hídricos de la Provincia de Santa Fe - Facultad de Ingeniería y Ciencias Hídricas de la Universidad Nacional del Litoral, 2006. Sistema de Alerta Hidrometeorológica de la Cuenca Inferior del Río Salado (1º Etapa); Informe Final; 1-104.

Miall, A.D., 1977. Lithofacies types and vertical profile models in braided river deposits: a summary, in: Miall, A.D. (Ed.), Fluvial Sedimentology. Can. Soc. Petrol. Geol. Mem., 5. pp. 597–604.

Miall, A.D., 2013. Fluvial Depositional System, Advances in Oil and Gas Exploration and Production. https://doi.org/10.1007/978-3-319-70335-0_9

Nichols, G.J., 1999. Sedimentology and Stratigraphy. Blackwell Publishing Ltd, London.

Paoli, C.U., Dondeynaz, C., Carmona-Moreno, C., 2015. Gestión integrada de crecidas. Guía y caso de estudio. Joint Research Centre, European Comm. Report EUR 27493 ES. https://doi.org/10.2788/997460

Pedersen, O.A., Brunetto, E., Zalazar, M.C., Chiaroto, L., 2022. Implementación de servidores de mapas para la prospección y análisis multi-proxy de eventos hidrológicos del Holoceno para la predicción de eventos futuros en la cuenca distal del Río Paraná, Entre Rios. XXI Congreso Geológico Argentino Puerto Madryn, Chubut - Marzo, 2022.

Pedraza, R., Torres, G., Morresi, M., Pusineri, G., Arbuet, M., 2017. Incorporación de la crecida de 1914 al análisis de frecuencias de crecidas, in: Gardiol, M., Morresi, M.V. (Eds.), Rio Salado: Un Aporte Al Conocimiento de La Crecida Extraordinaria de 1914. Santa Fe, pp. 133–150.

Ramos, V.A., Cristallini, E.O., Perez, D.J., 2002. The Pampean flat-slab of the Central Andes. J. South Am.

Earth Sci.

Richardson, T., Gilbert, H., Anderson, M., Ridgway, K.D., 2012. Seismicity within the actively deforming Eastern Sierras Pampeanas, Argentina. Geophys. J. Int. 188, 408–420. https://doi.org/10.1111/j.1365-246X.2011.05283.x

Roldán, J., Kröhling, D., 2021. Geoarqueología regional en ambientes fluviales y eólicos de un área de la Pampa Norte y del Chaco Austral (provincia de Santa Fe), in: Abstract Volume. IX Encuentro de Discusión Arqueológica Del Nordeste (EDAN). Instituto de Investigaciones Geohistóricas del Chaco, Resistencia, p. 83.

Saulo, A.C., Seluchi, M.E., Nicolini, M., 2004. A case study of a chaco low-level jet event. Mon. Weather Rev. 132, 2669–2683. https://doi.org/10.1175/MWR2815.1

Secretaría de Infraestructura y Política Hídrica de la República Argentina, 2022. Sistema Nacional de Información Hídrica | Argentina.gob.ar [WWW Document]. URL https://www.argentina.gob.ar/obras-publicas/hidricas/base-de-datos-hidrologica-integrada (accessed 5.20.22).

Seequent Ltd. (2022) Leapfrog Geo 4.0 Help, Contact surfaces. Seequent Ltd. https://help.leapfrog3d.com/Geo/4.0/en-GB/Content/geomodels/contact-surfaces.htm. Accessed 9 March 2022

Spalletti, P., Brea, D., 2002. Producción de sedimentos del noroeste argentino, in: XIX Congress on Natural Waters. Argentina, pp. 12–17.

St. George, S., Hefner, A.M., Avila, J., 2020. Paleofloods stage a comeback. Nat. Geosci. 13, 766–768. https://doi.org/10.1038/s41561-020-00664-2

Suprit, K., Kalla, A., Vijith, V., 2010. A GRASS-GIS-Based Methodology for Flash Flood Risk Assessment in Goa. Dona Paula, Goa: National Institute of Oceanography (CSIR) 1–74.

Thalmeier, M.B., Kröhling, D.M., Brunetto, E., 2021. The geomorphology and Late Quaternary sedimentary record of the Salado/Juramento fluvial megafan, Central Andes foreland basin (Chaco Plain, Argentina). Geomorphology 373. https://doi.org/10.1016/j.geomorph.2020.107495

Thorndycraft, V.R., Benito, G., Gregory, K.J., 2008. Fluvial geomorphology: A perspective on current status and methods. Geomorphology 98, 2–12. https://doi.org/10.1016/j.geomorph.2007.02.023

Veiga, G.D., Spalletti, L.A., Flint, S.S., 2007. Anatomy of a fluvial lowstand wedge: the Avilé Member of the Agrio Formation (Hauterivian) in central Neuquén Basin (NW Neuquén province), Argentina, in: Nichols, G., Williams, E., Paola, C. (Eds.), Sedimentary Environments, Processes and Basins, A Tribute to Peter Friend. International Association of Sedimentologists, New Jersey, Special Publications, 38, pp. 341–365.

Vera, C., Higgins, W., Amador, J., Ambrizzi, T., Garreaud, R., Gochis, D., Gutzler, D., Lettenmaier, D., Marengo, J., Mechoso, C.R., Nogues-Paegle, J., Silva Dias, P.L., Zhang, C., 2006. Toward a unified view of the American monsoon systems. J. Clim. 19, 4977–5000. https://doi.org/10.1175/JCLI3896.1

Vosselman, G., 2000. Slope based filtering of laser altimetry data. Int. Arch. Photogramm. Remote Sensing, Vol. 33, Part B3/2 33, 678–684. https://doi.org/10.1016/S0924-2716(98)00009-4

Vuille, M., Hardy, R., Keimig, F., Bradley, R.S., 1998. Atmospheric circulation anomalies associated with

1996/1997 summer precipitation events on Sajama Ice Cap, Bolivia. J. Geophys. Res. 103, 191–204.

Zhou, J., Lau, K.M., 1998. Does a monsoon climate exist over South America? J. Clim. 11, 1020–1040. https://doi.org/10.1175/1520-0442(1998)011<1020:DAMCEO>2.0.CO;2

Author Contributions: **Conceptualization Palaeohydrology**, O.P. and E.B; **Methodology,** O.P. (Multi-temporal teledetection analysis; UAV-Photogrammetry, Geodesy; GPR post-processing, GPR Sequence Stratigraphy; Implicit modelling; E.B. (Sequence stratigraphy; Geomorphometry), DK (Geomorphology; Sedimentology, Mineralogy), BT (Geomorphology; Sedimentology; Mineralogy); M.C.Z. (Geomorphometry); **Software,** O.P (GPR Leaf-frog; stratigraphic columns; M.C.Z (GRASS-GIS; Q-GIS; R; geomorphon and r.terrace.geom routine); B.T (GPR; GRASS-GIS; Q-GIS; stratigraphic columns); **Validation,** O.P. (multi-proxy Palaeohydrology), E.B (multi-proxy Palaeohydrology); **Formal Analysis,** O.P (Multi-temporal teledetection; GPR Sequence stratigraphy; Geodesy); E.B (Sequence stratigraphy; Sedimentology, Geomorphometry; instrumental and historical record analysis, D.K, (Stratigraphy; Geomorphology; historical record analysis) B.T; (Geomorphology); MCZ; (DEM statistics); **Resources,** O.P (UAV geodetic data); M.C.Z (DEMs derived products); B.T (GPR acquisition, Geomorphology, Sedimentology; Mineralogy); EB (Stratigraphy; GPR acquisition); D.K (Geomorphology, Stratigraphy; Sedimentology; GPR acquisition). **Data Curation,** M.C.Z; O.P: B.T; **Writing-Original Draft Preparation,** O.P; E.B, D.K; B.T.; M.C.Z; **Writing-Review & Editing**, E.B, D.K; O.P; B.T.; **Visualization**, **and Supervision**, E.B; D.K.; **Project Administration**, D.K.; **Funding Acquisition**, D.K

Journal Pre-proof

Journal Pre-proof

UAV	Field	RTK	GCP	Altitude m (AGL)	N° of Images	Flight date
P4PRO	Prospecting-scale	N/A	10	120	1587	7 Nov. 2018
P4RTK	Detail-scale	Enable	2	120	238	20 Nov. 2021
P4RTK	Detail-scale	Enable	2	100	321	20 Nov. 2021
P4RTK	Detail-scale	Enable	2	100	209	20 Nov. 2021

Journal Pre-proof

Journal Pre-proof

DEM	MIN DIF	MAX DIF	MEAN DIF.	σ	RMSE
MDE-Ar 30m	-0.4926	58,554	12,652	21,601	29,136
MDE-Ar 5m	-0.8120	12,272	0.4377	0.6419	10,873
Calibrated MDE-Ar 30m	-17578	42,577	12064	17791	22,186
Blended DEM 5m	-0.9230	14,292	0.6397	0.8219	11,962
VANT 1	-21501	-0.9303	12275	0.4858	13,307
VANT 2	-12300	0.7600	0.4453	0.6352	0.6202
VANT 3	44891	62,505	56587	0.6585	57,589
Calibrated VANT 1	-10800	0.1501	0.1844	0.4174	0.8687
Calibrated VANT 2	-0.6000	0.3000	0.1609	0.2922	0.4308
Calibrated VANT 3	-0.8623	11,707	0.3235	0.7020	0.7149

Journal Pre-proof

Journal Pre-proof

Flood indicator	Elevation (m.a.s.l.)	Local hydrometric level (m)	Discharge (m^3/s)	Estimated discharge excess (%)
yr. 2003 flood peak	24.37	13.28	3449	0.0
T1 top	24.3	13.21	3386	-1.8
T2 top	26.22	15.13	5109	48.1
T3 top	27.5	16.41	6257	81.4
Levee top	26.66	15.57	5503	59.6

Journal Pre-proof

Journal Pre-proof

Highlights

Combined geological and geodetic record enable reconstruction of extreme palaeofloods

Palaeoflood indicators are more realistic tracks for flooding hazard assessment

Geomorphometric routines calibrated in the field enable mapping maximum flood areas

Sequence fluvial stratigraphy is a good approach for palaeoflood succession studies

Journal Pre-proof

Journal Pre-proof

Declaration of interests

☒ The authors declare that they have no known competing financial interests or personal relationships that could have appeared to influence the work reported in this paper.

☐The authors declare the following financial interests/personal relationships which may be considered as potential competing interests:

Journal Pre-proof